PLASMA DYNAMICS

VI. PLASMAS AND CONTROLLED NUCLEAR FUSION*

A. Waves and Radiation

Academic and Research Staff

Prof. G. Bekefi
Prof. W. P. Allis
Prof. S. C. Brown
Prof. W. M. Manheimer
Prof. B. L. Wright
J. J. McCarthy
W. J. Mulligan
C. Oddou

Graduate Students

B. J. Becker
A. J. Cohen
L. Litzenberger
L. P. Mix, Jr.
L. D. Pleasance
G. L. Rogoff
C. E. Speck
N. E. Spithas
D. W. Swain
J. H. Vellenga

1. OBSERVATION OF ION ACOUSTIC WAVES IN HIGHLY IONIZED PLASMAS IN A MAGNETIC FIELD

This report gives preliminary data on the propagation of ion acoustic waves in highly ionized plasmas in a magnetic field. Measurements have been made using interferometric techniques in the PF 1 machine,[1] and indicate that the waves are dispersionless from well below to well above the ion-cyclotron frequency and obey the dispersion relation $\omega/k = (\gamma_e T_e + \gamma_i T_i/M_i)^{1/2}$. The source of the damping usually accompanying the wave is unknown, at the present time.

For the study of ion acoustic waves, the PF 1 is arranged with the modified Lisitano structure near one end of the system. A floating grid is placed approximately 4 cm

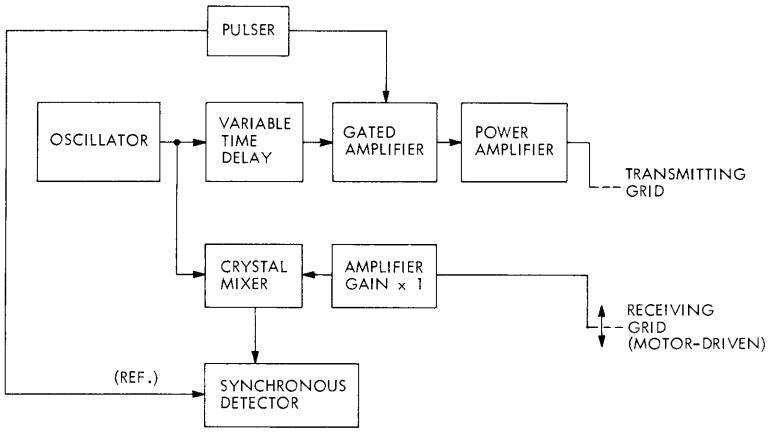

Fig. VI-1. Synchronous detection scheme used in the study of ion acoustic waves in PF 1.

*This work was supported by the U. S. Atomic Energy Commission (Contract AT(30-1)-3980).

from the structure. The transmitting and receiving grids are mounted on movable rods that pass through double O-ring seals at either end of the system. The receiving grid, located farthest from the plasma-generating structure, is equipped with a motor drive to provide uniform axial motion. The electronic equipment required for the launching and detection of ion acoustic waves is shown in Fig. VI-1. The variable time delay is used to adjust the phase of the transmitted signal so that the capacitive signal is 90° out of phase with the signal in the other arm of the interferometer. The amplifier in the receiver arm matches the plasma to the low-impedance crystal mixer. The output of the synchronous detector is used to drive the y axis of a recorder whose x axis is proportional to the receiver position. A typical trace for an Argon plasma is shown in Fig. VI-2.

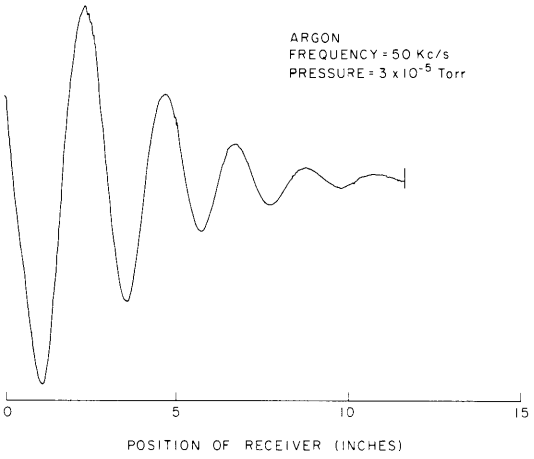

Fig. VI-2. Recorder trace of synchronous detector output as a function of receiver position.

The dispersion relations shown in Fig. VI-3 were obtained from two sets of data. The straight line is a plot of $\omega/k = (T_e/M_i)^{1/2}$, where $T_e = 4.12$ eV, as measured by a Langmuir probe in the Argon plasma. Silk's measurement of ion temperature in PF 2 indicates temperatures of ~0.3 eV (see Sec. VI-C.1). Although our data appear to indicate an increase in the phase velocity for $k_{Real} \geq 2$ cm^{-1}, the waves actually may be dispersionless for the following reason. As can be seen in Fig. VI-2, the wavelength of the wave tends to decrease with increasing distance from the transmitter, thereby indicating an axial temperature gradient toward the plasma source. Because the ratio of the imaginary to the real part of the wave vector is found to be essentially independent of frequency, the waves of longer wavelength can be observed over a greater distance before they damp out. At the present time, the length of the rod in the sliding seals puts an upper bound on the length of the measurement region. For wave vectors less than ~2 cm^{-1}, useful data are obtainable over the entire region. The damping for larger wave vectors reduces the length of the measuring region, thereby causing the average

measured wavelengths to fail to take into account the lower temperatures farther from the transmitter and leading to an apparent increase in the phase velocity. Future studies include the use of an axially movable probe to measure longitudinal variations in either density or electron temperature.

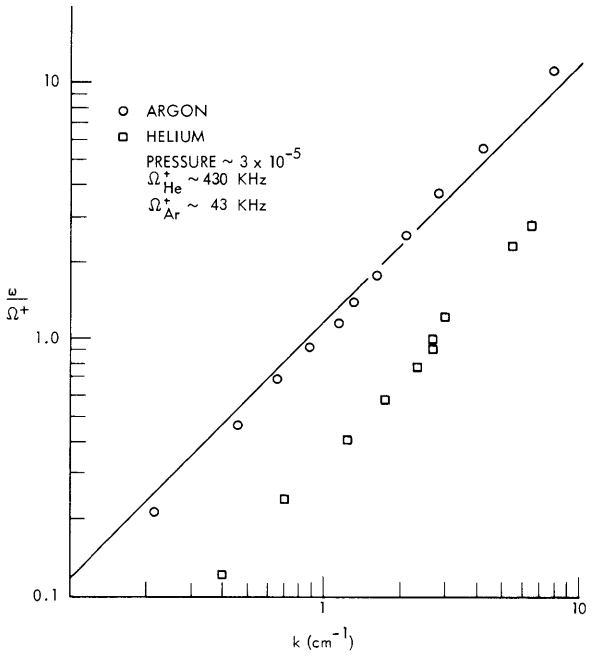

Fig. VI-3. Dispersion relations for Helium and Argon plasmas.

In order to verify these results, time-of-flight measurements have been made by using the techniques of Alexeff and Jones.[2] The results are in good agreement with those obtained by using the interferometric system. The change in slope of the distance vs time delay curve is also in at least qualitative agreement with the theory of a temperature gradient.

The damping is found to be significant. Although preliminary data indicate that the ratio of the imaginary part to the real part of the wave vector is approximately independent of frequency for a given set of plasma parameters, additional calculations indicate that neither ion nor electron Landau damping can account for the observed damping, unless significant drifts exist in the plasma or the ion temperatures in PF 1 differ appreciably from those measured by Silk in PF 2 (see Sec. VI-C. 1). Values of the damping ratio, k_i/k_r, vary from 0.12 to approximately 0.05 in Argon, and have been found to be typically 0.05 to 0.03 in Helium. The observed strong dependence of the damping on the plasma parameters makes it difficult to draw any conclusion about the dependence of damping on ion mass. We plan to monitor the plasma parameters

more closely in the future, in an attempt to determine the functional dependence of the damping distance on these parameters and to determine the damping mechanism.

L. P. Mix, Jr., L. Litzenberger, G. Bekefi

References

1. L. P. Mix, Jr., E. W. Fitzgerald, and G. Bekefi, Quarterly Progress Report No. 92, Research Laboratory of Electronics, M. I. T., January 15, 1969, p. 227.
2. I. Alexeff and W. D. Jones, Phys. Rev. Letters 15, 286 (1965).

2. NONLINEAR COUPLING OF THREE ION ACOUSTIC WAVES

Among the nonlinear effects that are possible in plasmas is the exchange of energy among three or more waves, commonly known as mode coupling. In order for this energy exchange to occur among, say, three waves with frequencies ω_1, ω_2, and ω_3, and with wave vectors $\vec{k}_1$, $\vec{k}_2$, $\vec{k}_3$, the following selection rules must be obeyed exactly (or nearly exactly):

$$\omega_1 = \omega_2 + \omega_3 \tag{1}$$

$$\vec{k}_1 = \vec{k}_2 + \vec{k}_3. \tag{2}$$

In order for the energy exchange to be observable in the laboratory, it is also necessary that the distance over which appreciable energy exchange occurs, henceforth called the interaction length L, be less than or of the order of the largest dimension of the plasma that is available.

We have observed ion acoustic waves (see Sec. VI-A. 1) in the plasma described in a previous report.[1] These waves do not exhibit dispersion, at least at low enough frequencies; hence, satisfaction of (1) automatically ensures satisfaction of (2) when the wave vectors have the same direction. In order to determine the feasibility of studying nonlinear coupling among three of these waves in our plasma, we calculated some interaction lengths on the basis of the moment equations, in a manner similar to that of Sugihara.[2] We present this calculation here; the results are encouraging.

We assume that there is no damping of the ion acoustic waves of interest,[3] that the frequencies of interest are much less than the ion plasma frequency, ω_{pi}, so that there is quasi-neutrality at every instant of time ($(\nabla \cdot \vec{E}) = 0$) and so that the instantaneous electron and ion velocities are equal to one another at every instant. The parameters of the wave-free plasma are assumed to be spatially and temporally independent. Finally, we assume that there are no DC drifts and no DC electric fields in the plasma and that the ions are "cold" so that there is no ion pressure.

The particle and momentum conservation equations (with source terms set equal to

zero) for both the electron gas and the ion gas are employed. We assume that conditions are such that the Lorentz force terms in the momentum-conservation equations can be neglected. Each quantity in the equations is expanded in the normal manner in terms of its DC component, denoted here by an upper-case letter, and its AC component, denoted by a lower-case letter, except for the AC electric field which is denoted by $\vec{E}$. Instead, however, of retaining only terms of order one or zero in AC components as in the linear theory, we now retain terms of second order also.

The following set of equations results, in which subscript e denotes electron, subscript i denotes ion, m is the electron mass, M is the ion mass, e is the charge of the electron ($e > 0$), and terms nonlinear in AC components are kept on the right side of the equation:

$$\frac{\partial n_{e,i}}{\partial t} + N_{e,i} \nabla \cdot \vec{v}_{e,i} = -\nabla \cdot (n_{e,i} \vec{v}_{e,i}) \tag{3}$$

$$\frac{\partial \vec{v}_e}{\partial t} + \frac{e}{m} \vec{E} + \frac{1}{mN_e} \nabla p_e = -(\vec{v}_e \cdot \nabla)\vec{v}_e + \frac{n_e}{N_e^2 m} \nabla p_e \tag{4}$$

$$\frac{\partial \vec{v}_i}{\partial t} - \frac{e}{M} \vec{E} = -(\vec{v}_i \cdot \nabla)\vec{v}_i. \tag{5}$$

Eliminating the electric field between (4) and (5) and dropping terms that are less by a factor m/M than other terms in the combined equation, we get

$$\frac{\partial v_i}{\partial t} + \frac{1}{MN_e} \nabla p_e = -(\vec{v}_i \cdot \nabla)\vec{v}_i + \frac{n_e}{N_e^2 M} \nabla p_e. \tag{6}$$

Let us assume adiabatic pressure variations in the electron gas. The AC pressure can be eliminated in favor of the AC density in (6) in this way, thereby yielding the following equation

$$\frac{\partial \vec{v}_i}{\partial t} + \frac{P_e \gamma}{N_e^2 M} \nabla n_e = -(\vec{v}_i \cdot \nabla)\vec{v}_i + \frac{n_e P_e \gamma}{N_e^3 M} \nabla n_e - \frac{P_e \gamma(\gamma-1)}{2MN_e^3} \nabla (n_e)^2, \tag{7}$$

where γ is the ratio of the specific heats for the electron gas.

The subscripts can be dropped in (7), because of some assumptions that we have made. By assuming that $P = NK_B T$, that is, that the ideal gas law holds for the wave-free electron gas, defining

$$V_s^2 = \frac{\gamma K_B T}{M} \tag{8}$$

and taking the divergence, (7) becomes

$$\frac{\partial}{\partial t}\nabla\cdot\vec{v} + V_s^2\nabla^2\frac{n}{N} = -\nabla\cdot[(\vec{v}\cdot\nabla)\vec{v}] + \frac{2-\gamma}{2}V_s^2\nabla^2\left(\frac{n}{N}\right)^2. \tag{9}$$

Eliminating $\frac{\partial}{\partial t}\nabla\cdot\vec{v}$ between (9) and the time derivative of (3), and introducing the normalized density

$$n' = \frac{n}{N}, \tag{10}$$

we arrive at the following equation:

$$\frac{\partial^2 n'}{\partial t^2} - V_s^2\nabla^2 n' = \nabla\cdot[(\vec{v}\cdot\nabla)\vec{v}] - \left(\frac{2-\gamma}{2}\right)V_s^2\nabla^2(n')^2 - \frac{\partial}{\partial t}\nabla\cdot(n'\vec{v}). \tag{11}$$

Note that neglecting the nonlinear terms on the right side of (11) leads to the familiar wave equation for ion acoustic waves with the phase velocity equal to $\sqrt{\gamma K_B T/M}$. The nonlinear terms on the right side of (11) and (3) are the "sources" responsible for the nonlinear wave interactions.

Instead of working with (11) we choose to work with (9), with the divergence operator removed, namely

$$\frac{\partial\vec{v}}{\partial t} + V_s^2\nabla n' = -(\vec{v}\cdot\nabla)\vec{v} + \frac{2-\gamma}{2}V_s^2\nabla(n')^2. \tag{12}$$

The next step is to insert the following expansions into (3) and (12):

$$n' = \frac{n}{N} = \sum_{\ell=1,2,3}[C_\ell(t)\exp(j\psi_\ell) + C_\ell^*(t)\exp(-j\psi_\ell)] \tag{13}$$

$$v' = \frac{v}{V_s} = \sum_{\ell=1,2,3}[B_\ell(t)\exp(j\psi_\ell) + B_\ell^*(t)\exp(-j\psi_\ell)], \tag{14}$$

where

$$\psi_\ell = \omega_\ell t - k_\ell x. \tag{15}$$

In other words, consider three plane ion acoustic waves (ℓ=1, 2, 3) propagating colinearly in the +x direction in the plasma and hence having their velocity vectors oriented in the x direction. Recall that all damping mechanisms have been ignored; however, the complex amplitudes of the waves will still vary slowly in time, because of the nonlinear terms in (3) and (12).

Let us invoke exact phase matching; that is, $\psi_1 = \psi_2 + \psi_3$ because selection rules (1)

and (2) must be obeyed if the three ion acoustic waves are to exchange energy. We drop all "nonresonant" terms, that is, terms whose ψ_ℓ dependence is neither $\exp(\pm i\psi_1)$, $\exp(\pm i\psi_2)$, nor $\exp(\pm i\psi_3)$ from the equations obtained by inserting (13) and (14) into (3) and (12) and by using $\psi_1 = \psi_2 + \psi_3$. These "nonresonant" terms do not contribute to the interaction of the three waves in question.

We assume that the AC quantities are large enough to warrant having kept second-order terms in the moment equations but not too large, so that the linear dispersion relation $\omega/k = V_s$ can still be expected to hold.

Equating the terms on the left side of (3) that are periodic in ψ_1 to terms on the right side that have the same period $\psi_1 = \psi_2 + \psi_3$, and proceeding similarly for ψ_2 and ψ_3, we get the following set of equations and the complex conjugates of these equations:

$$\frac{1}{\omega_1}\frac{dC_1}{dt} + jC_1 - jB_1 = j[C_2B_3 + C_3B_2] \tag{16}$$

$$\frac{1}{\omega_2}\frac{dC_2}{dt} + jC_2 - jB_2 = j\left[C_3^*B_1 + C_1B_3^*\right] \tag{17}$$

$$\frac{1}{\omega_3}\frac{dC_3}{dt} + jC_3 - jB_3 = j\left[C_1B_2^* + C_2^*B_1\right]. \tag{18}$$

Equating proper terms in (12), we get the following set of equations and the complex conjugates of these equations:

$$\frac{1}{\omega_1}\frac{dB_1}{dt} + jB_1 - jC_1 = j[B_2B_3 - (2-\gamma)C_2C_3] \tag{19}$$

$$\frac{1}{\omega_2}\frac{dB_2}{dt} + jB_2 - jC_2 = j\left[B_3^*B_1 - (2-\gamma)C_3^*C_1\right] \tag{20}$$

$$\frac{1}{\omega_3}\frac{dB_3}{dt} + jB_3 - jC_3 = j\left[B_1B_2^* - (2-\gamma)C_1C_2^*\right]. \tag{21}$$

Adding (16) and (19), (17) and (20), (18) and (21), and realizing from (3) that $B_\ell = C_\ell$ (ℓ=1, 2, 3) to first order, we get a set of coupled equations that describe the time rate of change of the normalized AC density amplitudes or of the normalized AC velocity amplitudes. We are more interested, however, in the AC electric fields than in the AC densities or the AC velocities; hence, we shall not write down these equations for the C's and B's. Instead, if

$$E = \sum_{\ell=1,\,2,\,3} [\mathscr{E}_\ell(t)\exp(j\psi_\ell) + \mathscr{E}^*_\ell(t)\exp(-j\psi_\ell)], \tag{22}$$

it is easy to get the following relation between $\mathscr{E}_\ell$ and C_ℓ by neglecting nonlinear terms in (5) and (6), eliminating $\partial\vec{v}_i/\partial t$ between these two equations, and using the linearized expression for p in terms of n coming from our assumption of adiabaticity:

$$C_\ell = -j\frac{e}{M}\frac{1}{\omega_\ell V_s}\mathscr{E}_\ell. \tag{23}$$

Consequently,

$$\frac{d\mathscr{E}_1}{dt} = \left[\left(\frac{e}{MV_s}\right)\left(\frac{\gamma+1}{2}\right)\left(\frac{\omega_1^2}{\omega_2\omega_3}\right)\right]\mathscr{E}_2(t)\,\mathscr{E}_3(t) \tag{24}$$

$$\frac{d\mathscr{E}_2}{dt} = \left[-\left(\frac{e}{MV_s}\right)\left(\frac{\gamma+1}{2}\right)\left(\frac{\omega_2^2}{\omega_1\omega_3}\right)\right]\mathscr{E}_1(t)\,\mathscr{E}^*_3(t) \tag{25}$$

$$\frac{d\mathscr{E}_3}{dt} = \left[-\left(\frac{e}{MV_s}\right)\left(\frac{\gamma+1}{2}\right)\left(\frac{\omega_3^2}{\omega_1\omega_2}\right)\right]\mathscr{E}_1(t)\,\mathscr{E}^*_2(t). \tag{26}$$

These, then, are the equations describing the temporal variations of the complex amplitudes of the electric fields of the three waves that are interacting. They are commonly called the coupled-mode equations.

We can generalize (24), (25), and (26) by replacing the terms in square brackets with the matrix elements V_{123}, V_{213}, and V_{312}, respectively. That these generalized equations actually hold for the nonlinear coupling of any three plane, undamped waves propagating colinearly in an infinite homogeneous medium has been shown on the basis of quite general principles by Bloembergen[4] among others. The matrix elements contain all of the detailed physical characteristics of the plasma or other medium, information about the relative polarization of the three waves, their frequencies and propagation constants. The task of computing expressions for the matrix elements, which is essentially the task that we have been undertaking for the special case of three ion acoustic waves, is often one of considerable difficulty. Furthermore, if the waves are dispersive, often it is not possible to satisfy selection rules (1) and (2), in which case three-wave coupling cannot even take place. In that event, it might still be possible to couple four or more waves.

It is wise at this point, before proceeding to solve (24), (25), and (26), to check that the total time-averaged energy density of these three waves is conserved, as it should be, on

account of the assumption of no damping. To do this we multiply (24) by $\mathscr{E}_1^*$ and the complex conjugate of (24) by $\mathscr{E}_1$; we then add the two equations. We find we have an equation for $\frac{d}{dt}\left(\frac{|\mathscr{E}_1|^2}{\omega_1^2}\right)$. Proceeding in the same manner with (25) and (26), and using $\omega_1, = \omega_2 + \omega_3$, we find

$$\frac{|\mathscr{E}_1|^2}{\omega_1^2} + \frac{|\mathscr{E}_2|^2}{\omega_2^2} + \frac{|\mathscr{E}_3|^2}{\omega_3^2} = \text{constant in time.} \tag{27}$$

We now calculate the total time-averaged energy density $\langle U \rangle$ for each wave from

$$\langle U \rangle = \frac{1}{4}\,\epsilon_o |\mathscr{E}|^2 \frac{\partial}{\partial \omega}(\omega K_L), \tag{28}$$

where K_L is the linear dielectric coefficient. For an ion acoustic wave of frequency ω much less than the ion plasma frequency ω_{pi},

$$K_L \approx -\frac{\omega_{pi}^2}{\omega^2} + \frac{1}{k^2 L_D^2}, \tag{29}$$

where L_D is the electron Debye length. Performing the differentiation required by (28), we obtain

$$\langle U \rangle = \frac{1}{4}\,\epsilon_o |\mathscr{E}|^2 \frac{\omega_{pi}^2}{\omega^2}. \tag{30}$$

Hence the total time-averaged energy density for all three waves is

$$\langle U_T \rangle = \frac{1}{4}\,\epsilon_o \omega_{pi}^2 \left[\frac{|\mathscr{E}_1|^2}{\omega_1^2} + \frac{|\mathscr{E}_2|^2}{\omega_2^2} + \frac{|\mathscr{E}_3|^2}{\omega_3^2}\right]. \tag{31}$$

Comparing (27) and (31), we see that energy is conserved.

Let us proceed to solve (24), (25), and (26). It is convenient to express each complex electric field amplitude $\mathscr{E}_\ell$ (ℓ=1, 2, 3) as

$$\mathscr{E}_\ell = A_\ell(t)\,\exp[j\phi_\ell(t)], \tag{32}$$

where, A_ℓ and ϕ_ℓ are real quantities. Inserting this into (24), (25), and (26), and

separating the equations into equations for real and imaginary parts, we arrive at separate equations for dA_ℓ/dt and $d\phi_\ell/dt$ (ℓ=1, 2, 3). The equations for the dA/dt follow.

$$\frac{dA_1}{dt} = \left(\frac{e}{MV_s}\right)\left(\frac{\gamma+1}{2}\right)\left(\frac{\omega_1^2}{\omega_2\omega_3}\right) A_2A_3 \cos\delta \tag{33}$$

$$\frac{dA_2}{dt} = -\left(\frac{e}{MV_s}\right)\left(\frac{\gamma+1}{2}\right)\left(\frac{\omega_2^2}{\omega_1\omega_3}\right) A_1A_3 \cos\delta \tag{34}$$

$$\frac{dA_3}{dt} = -\left(\frac{e}{MV_s}\right)\left(\frac{\gamma+1}{2}\right)\left(\frac{\omega_3^2}{\omega_1\omega_2}\right) A_1A_2 \cos\delta, \tag{35}$$

where

$$\delta = \phi_1 - \phi_2 - \phi_3. \tag{36}$$

Using (33) to replace A_2A_3 in the equation for $d\phi_1/dt$, (34) to replace A_3A_1 in the equation for $d\phi_2/dt$, and (35) to replace A_1A_2 in the equation for $d\phi_3/dt$, we readily find that

$$\frac{d\delta}{dt} = -(\tan\delta)\frac{d}{dt}\ln(A_1A_2A_3) \tag{37}$$

so that

$$A_1A_2A_3 \sin\delta = \text{constant in time} = a. \tag{38}$$

It is relatively easy to show from (30), (32), (33), (34), and (35) that

$$\frac{\langle U_1\rangle}{\omega_1} + \frac{\langle U_2\rangle}{\omega_2} = \text{constant in time} \tag{39}$$

$$\frac{\langle U_1\rangle}{\omega_1} + \frac{\langle U_3\rangle}{\omega_3} = \text{constant in time} \tag{40}$$

$$\frac{\langle U_2\rangle}{\omega_2} - \frac{\langle U_3\rangle}{\omega_3} = \text{constant in time.} \tag{41}$$

These relations are commonly referred to as the Manley-Rowe relations, well-known in the theory of parametric amplifiers. We realize that these relations describe the creation and destruction of quanta because $\langle U_\ell\rangle/\omega_\ell$ is proportional to the number of

quanta per unit volume in the ℓ^{th} wave (ℓ=1, 2, 3). For example, (39) and (40) say that when a quantum at frequency ω_1 disappears, a quantum appears at each of the frequencies ω_2 and ω_3.

From (38) we get

$$\cos\delta = \pm\sqrt{1 - \frac{a^2}{A_1^2A_2^2A_3^2}}.$$

Using this in (33), (34), and (35), and using $n_\ell = A_\ell^2/\omega_\ell^3$ (ℓ=1, 2, 3) (42) to make a change of variables in these equations, we arrive at the following equations:

$$\frac{dn_1}{dt} = +V\sqrt{n_1n_2n_3 - \Gamma^2} \tag{43}$$

$$\frac{dn_2}{dt} = -V\sqrt{n_1n_2n_3 - \Gamma^2} \tag{44}$$

$$\frac{dn_3}{dt} = -V\sqrt{n_1n_2n_3 - \Gamma^2}, \tag{45}$$

where

$$V = \pm\frac{e}{MV_s}(\gamma+1)\sqrt{\omega_1\omega_2\omega_3} \tag{46}$$

$$\Gamma^2 = n_1n_2n_3\sin^2\delta = \text{constant in time.} \tag{47}$$

V has the same sign as cos δ.

We realize from the Manley-Rowe relations and the definition of n_ℓ and of A_ℓ that

$$n_1(t) + n_2(t) = n_1(0) + n_2(0) = m_a \tag{48}$$

$$n_1(t) + n_3(t) = n_1(0) + n_3(0) = m_b \tag{49}$$

$$n_2(t) - n_3(t) = n_2(0) - n_3(0) = m_c. \tag{50}$$

Therefore,

$$\frac{dn_1}{dt} = V\sqrt{n_1(n_1-m_a)(n_1-m_b) - \Gamma^2}. \tag{51}$$

But

$$n_1(n_1-m_a)(n_1-m_b) - \Gamma^2 = (n_1-n_{1a})(n_1-n_{1b})(n_1-n_{1c}), \tag{52}$$

where n_{1a}, n_{1b}, and n_{1c} are the three roots of this third-order polynomial, $n_{1c} \geq n_{1b} \geq n_{1a} \geq 0$. Therefore

$$\frac{dn_1}{dt} = V\sqrt{(n_1-n_{1a})(n_1-n_{1b})(n_1-n_{1c})}. \tag{53}$$

We integrate (53) from time t_o to time t and make another change of variables, namely[4]

$$y(t) = \sqrt{\frac{n_1(t) - n_{1a}}{n_{1b} - n_{1a}}}. \tag{54}$$

Also, let

$$\Lambda = \sqrt{\frac{n_{1b} - n_{1a}}{n_{1c} - n_{1a}}}. \tag{55}$$

The result is

$$\int_{y(t_o)}^{y(t)} \frac{dy}{\sqrt{(1-y^2)(1-\Lambda^2y^2)}} = \sqrt{n_{1c} - n_{1a}}\,\frac{V}{2}\,(t-t_o). \tag{56}$$

If we now choose t_o so that

$$y(t_o) = \sqrt{\frac{n_1(t_o) - n_{1a}}{n_{1b} - n_{1a}}} = 0, \tag{57}$$

the integral on the left side of (56) is the elliptic integral of the first kind with modulus Λ. Hence

$$y(t) = \mathrm{sn}\left[\int_0^{y(t)} \frac{dy}{\sqrt{(1-y^2)(1-\Lambda^2y^2)}}\right] = \mathrm{sn}\left[\sqrt{n_{1c} - n_{1a}}\,\frac{V}{2}\,(t-t_o); \Lambda\right]. \tag{58}$$

Using (48), (49), (50), (54), and (58), we get

$$n_1(t) = n_{1a} + (n_{1b}-n_{1a})\,\mathrm{sn}^2\left[\sqrt{n_{1c} - n_{1a}}\,\frac{|V|}{2}\,(t-t_o); \Lambda\right] \tag{59}$$

$$n_2(t) = n_1(0) + n_2(0) - n_{1a} - (n_{1b}-n_{1a})\,\mathrm{sn}^2\left[\sqrt{n_{1c} - n_{1a}}\,\frac{|V|}{2}\,(t-t_o); \Lambda\right] \tag{60}$$

$$n_3(t) = n_1(0) + n_3(0) - n_{1a} - (n_{1b}-n_{1a})\, sn^2\left[\sqrt{n_{1c} - n_{1a}}\,\frac{|V|}{2}(t-t_o); \Lambda\right]. \tag{61}$$

Equations 59-61 fully describe the interaction of the three ion acoustic waves in general. Let us look at some cases of specific initial conditions and calculate some interaction lengths. We expect that an interaction time coming out of the theory discussed above is related to the interaction length, L, that we seek simply by the phase velocity V_s of these waves, that is, $L = (V_s)$(Interaction Time).

CASE 1. $n_2(0) \gg n_3(0) > n_1(0) = 0$

Now $\Gamma = 0$, $m_a = n_2(0)$, $m_b = n_3(0)$, and $m_c = n_2(0) - n_3(0)$. Using ((52), we see that $n_{1a} = 0$, $n_{1b} = n_3(0)$, and $n_{1c} = n_2(0)$. Therefore, $\Lambda \ll 1$; and we are justified in neglecting the $\Lambda^2 y^2$ term in the denominator of the integrand in (56), provided that y does not become too large over the range of integration. We can integrate the resulting expression to get

$$\pm \sin^{-1} y(t) = \frac{V}{2}(t-t_o)\sqrt{n_2(0)}, \tag{62}$$

recalling that t_o is chosen so that $y(t_o) = 0$. Because $|y| \leq 1$ always, we were justified in dropping $\Lambda^2 y^2$. We realize from (57) that $n_1(t_o) = n_{1a} = 0$, which tells us that $t_o = 0$. Hence, using (54), we obtain

$$n_1(t) = n_3(0)\sin^2\left(\frac{|V|}{2}\sqrt{n_2(0)}\; t\right). \tag{63}$$

We conclude that wave 1 grows from its value of zero at x = 0 to its maximum value of $n_3(x=0)$ in an interaction length

$$L = \pi\,\frac{MV_s^2}{e}\,\frac{1}{\gamma+1}\,\frac{1}{\sqrt{\omega_1\omega_2\omega_3}}\,\frac{1}{\sqrt{n_2(0)}}. \tag{64}$$

Recall that

$$n_2(t) = \frac{[A_2(t)]^2}{\omega_2^3} = \frac{|\mathscr{E}_2(t)|^2}{\omega_2^3}.$$

Therefore

$$L = \frac{K_B T}{e|\mathscr{E}_2(x=0)|}\,\frac{\gamma}{\gamma+1}\,\frac{\omega_2}{\sqrt{\omega_1\omega_3}}\,\pi. \tag{65}$$

By driving wave 2 sufficiently hard and by choosing ω_2 and ω_3 wisely, we believe we shall be able to make L appreciably less than the length of the plasma at our disposal because the electron temperature, T, for this plasma is of the order of a few electron volts. Note that sinusoidal variations of energy densities with distance are expected for this particular set of initial conditions; note also the dependence of the maximum of n_1 on $n_3(0)$ and the dependence of L on $|\mathscr{E}_2(x=0)|$ and on the frequencies. Comparison between theory and experiment can be made on this level, once the interaction of the waves is observed.

CASE 2. $n_1(0) \gg n_2(0) > n_3(0) = 0$

Now $\Gamma = 0$, $m_a = n_1(0) + n_2(0)$, $m_b = n_1(0)$, and $m_c = n_2(0)$. Equation 52 tells us that $n_{1a} = 0$, $n_{1b} = n_1(0)$, and $n_{1c} = n_1(0) + n_2(0)$.

$$\therefore \quad n_1(t) = n_1(0)\ \mathrm{sn}^2\left[\sqrt{n_1(0) + n_2(0)}\ \frac{|V|}{2}\ (t-t_o); \Lambda\right] \tag{66}$$

$$n_3(t) = n_1(0)\left\{1 - \mathrm{sn}^2\left[\sqrt{n_1(0) + n_2(0)}\ \frac{|V|}{2}\ (t-t_o); \Lambda\right]\right\} \tag{67}$$

$$n_3(0) = 0 \Longrightarrow 1 = \mathrm{sn}^2\left[\sqrt{n_1(0) + n_2(0)}\ \frac{|V|}{2}\ t_o; \Lambda\right]. \tag{68}$$

It is the complete elliptic integral of the first kind that has sn = 1; that is,

$$\mathrm{sn}[K(\Lambda)] = \mathrm{sn}\left[\int_0^1 \frac{dy}{\sqrt{(1-y^2)(1-\Lambda^2 y^2)}}\right] = 1. \tag{69}$$

Hence

$$t_o = \frac{2}{\sqrt{n_1(0) + n_2(0)}}\ \frac{1}{|V|}\ K(\Lambda). \tag{70}$$

$$\Lambda' = \sqrt{1 - \Lambda^2} = \sqrt{\frac{n_2(0)}{n_1(0) + n_2(0)}} \ll 1.$$

For this limit,

$$K(\Lambda) \approx \ln_e\left(\frac{4}{\Lambda'}\right).$$

Hence

$$t_o \approx \frac{2}{\sqrt{n_1(0) + n_2(0)}} \frac{1}{|V|} \ln_e \left[4 \sqrt{\frac{n_1(0) + n_2(0)}{n_2(0)}} \right]. \tag{71}$$

Recall that $n_1(t_o) = n_{1a} = 0$; hence, t_o is the time it takes for the energy in wave 1 to go from its initial value to zero. Consequently, we may interpret t_o as the interaction time; and

$$L \approx \frac{K_B T}{e|\mathcal{E}_1(x=0)|} \frac{2\gamma}{\gamma + 1} \frac{\omega_1}{\sqrt{\omega_2 \omega_3}} \ln_e \left(4 \sqrt{\frac{n_1(0)}{n_2(0)}} \right). \tag{72}$$

Again, results are encouraging. It is interesting to note that $L \to \infty$ as $n_2(0) \to 0$. Hence it appears that there can be no interaction among waves 1, 2, and 3 when wave 1 is externally excited, unless there is some initial energy in wave 2, either from the thermal spectrum or by externally exciting this wave also.

CASE 3. $n_2(0) \gg n_1(0) > n_3(0) = 0$.

Now $\Gamma = 0$, $m_a = n_1(0) + n_2(0)$, $m_b = n_1(0)$, and $m_c = n_2(0)$. Equation 52 tells us that $n_{1a} = 0$, $n_{1b} = n_1(0)$, and $n_{1c} = n_1(0) + n_2(0)$. Therefore, $\Lambda \ll 1$; and we may drop the $\Lambda^2 y^2$ term in the denominator of (56) under the assumption that y does not become too large in the region of integration. Consequently,

$$\pm \sin^{-1} y(t) = \sqrt{n_1(0) + n_2(0)} \frac{V}{2} (t - t_o). \tag{73}$$

We recall that t_o is chosen so that $y(t_o) = 0$. We see that $|y| \leq 1$ always, so dropping $\Lambda^2 y^2$ is justified. Therefore

$$n_1(t) = n_1(0) \sin^2 \left[\sqrt{n_1(0) + n_2(0)} \frac{|V|}{2} (t - t_o) \right] \tag{74}$$

$$L \approx \frac{K_B T}{e|\mathcal{E}_2(x=0)|} \frac{\gamma}{\gamma + 1} \frac{\omega_2}{\sqrt{\omega_1 \omega_3}} \pi. \tag{75}$$

Again, the results are encouraging.

We plan to investigate the nonlinear coupling of three ion acoustic waves, once we have completed the examination of these waves in the linear regime.

L. N. Litzenberger, G. Bekefi

References

1. L. P. Mix, Jr., E. W. Fitzgerald, and G. Bekefi, "Construction and Properties of a Collisionless, Quiescent Plasma Facility (PF 1)," Quarterly Progress Report No. 92, Research Laboratory of Electronics, M. I. T., January 15, 1969, p. 227.
2. R. Sugihara, "Interaction between an Electromagnetic Wave, Plasma Waves, and an Ion Acoustic Wave," Phys. Fluids 11, 178 (1968).
3. Introducing damping into the picture leads to a threshold condition for the onset of the coupling. We do not wish to concern ourselves with this in this report.
4. N. Bloembergen, Nonlinear Optics (W. A. Benjamin, Inc., New York, 1965).

3. RELATION BETWEEN MOVING STRIATIONS AND ION ACOUSTIC WAVES

Introduction

When an experimenter runs a glow discharge in one of the noble gases, he often observes self-excited moving or standing striations of large amplitude.[1] The characteristics of these striations change with gas species, current, pressure, and tube size. At lower pressures, it is sometimes possible to obtain a uniform positive column in which low-amplitude striations can be excited by external means. In most theories of striations it is necessary to take into account that the wave has associated with its passage down the tube a time and spatially varying ionization frequency.[2] Most of these theories have been formulated to account for high-pressure behavior (pressures of the order of 1 Torr), and so they might be inapplicable at low pressure.

On the other hand, ion acoustic waves are predicted by simple theory to occur in uniform homogeneous plasmas. The behavior of these waves is much like that of sound waves in neutral gases. They have a constant phase velocity, and they are purely longitudinal waves. At low pressures, these waves have often been observed, by either externally exciting them or observing them as self-excited waves when they are in an unstable regime. Considerable theoretical and experimental work has been done on these waves, and they are believed to be fairly well understood.[3,4]

It has been speculated that these waves might have some connection with each other, and indeed ion acoustic theory has sometimes been used to predict some of the properties of striations successfully.[5] This report will present an analytical theory that predicts the behavior of both kinds of waves, reducing in appropriate limits to the simple theories of ion acoustic and ionization waves. In order to treat the problem analytically, certain simplifications have been made which in reality are not justified. The qualitative behavior of the two waves is not affected, however, and the theory gives a clear picture of the relation between the waves.

First, the equations of motion for the ions will be derived. Then the electron

equations will be discussed. Finally, the dispersion relation for the waves will be discussed and a comparison will be made with experiment. The assumptions are made throughout to try to model the positive column of a low-pressure glow discharge.

Equations of Motion for the Ions

Assume that the ions have a Maxwellian velocity distribution and that the moment equations can be used to describe their behavior. Then the conservation of particles and conservation of mementum equations are

$$\frac{\partial N}{\partial t} + \text{div}\,(N\vec{V}) = R \tag{1}$$

$$MN\,\frac{d\vec{V}}{dt} = qN\vec{E} - \text{grad}\,p - MN\nu_+\vec{V} - M\vec{V}R, \tag{2}$$

where R is the rate at which particles are created per sec per cm^3. Equation 2 has a momentum transfer term, because of this creation term, since it assumes that the particles are created from neutral gas atoms which have zero drift velocity. Assume that $R = Z_iN$, where Z_i = ionization frequency, and N = electron (and ion) density. In this derivation I make the assumption that the electron and ion densities are approximately equal everywhere, with only a negligible difference between them giving rise to the time-variant electric field that exists in the plasma. Now let N, $\vec{V}$, $\vec{E}$, and Z have steady-state and time-variant parts of the form $X = X + xe^{i(kz-\omega t)}$. Also, neglect the grad p term in the momentum equations, since it is a small term for the relatively low-temperature ions. The z axis is along the axis of the tube, with z increasing from anode to cathode. The steady-state equations become

$$\vec{V} = \frac{q\vec{E}}{M(\nu_+ + Z_i)} \tag{3}$$

$$\frac{1}{r}\,\frac{\partial}{\partial r}\,(rNV_r) = Z_iN. \tag{4}$$

Equation 3 simply gives the drift velocity in the DC field. Equation 4 states that the creation rate must equal the loss rate as a result of radial transport to the walls (recombination can be neglected for sufficiently low density).

After linearizing the time-dependent equations, they become

$$-i(\omega - kV)\,n + ikNv = z_iN \tag{5}$$

$$-iMN(\omega - kV)\,v = qNe - MN(\nu_+ + Z_i)\,v - MNVz_i, \tag{6}$$

where v, n, e, and z_i are the time-varying components of the axial ion drift velocity, density, electric field, and ionization frequency, respectively. Here use has also been made of (3) and (4). Let $\omega' = \omega - kV$, and eliminate v from (5) and (6).

$$-i\omega' \frac{n}{N} + \frac{ikqE}{M(-i\omega'+\nu_+ + Z_i)} \frac{e}{E} = \left[1 + \frac{ikV}{(-i\omega'+\nu_+ + Z_i)}\right] z_i. \tag{7}$$

Equation 7 gives a relationship between the three variables n, e, and z_i. To get a dispersion relation, it is necessary to examine the electron equations, which will be done eventually.

The derivation of (7) has proceeded along more or less standard lines, with the addition of the z_i term. If we set $z_i = 0$, and assume $Z_i \ll \nu_+$, we obtain

$$-i\omega' \frac{n}{N} + \frac{ikqE}{M(-i\omega'+\nu_+)} \frac{e}{E} = 0. \tag{8}$$

This is the usual ion equation of motion which is obtained in the derivations of ion acoustic waves at low frequencies ($\omega \ll \omega_{pi}$, the ion plasma frequency).

If we assume ω' and $Z_i \ll \nu_+$, then

$$-i\omega' \frac{n}{N} + ikV \frac{e}{E} = \left(1 + \frac{ikV}{\nu_+}\right) z_i. \tag{9}$$

Equation 9 corresponds to Pekarek's equations of ion motion in his theory of striations.[2] Neglecting ω' relative to ν_+ corresponds to neglecting the ion inertia term in the momentum equation. When this is done, we have gone from a wave type of equation (as for ion acoustic waves at low pressure) to a diffusion type of equation (as used by Pekarek for striations at high pressures).

The electron equations turn out to be independent of ω. Therefore, since ω' appears twice in (7) and (8), but only once in (9), the last equation will only have one root $\omega(k)$, while the other equations will have 2 roots. For (8), these roots are the two ion acoustic modes propagating in opposite directions. In Eq. 7, one root will be very close to one of the ion-acoustic mode solutions of Eq. 8. The other root will be significantly modified by the right-hand side of (7), going to the other ion acoustic mode for large values of k and to striationlike behavior for small k.

Equations of Motion for the Electrons

For the electrons, I shall make the assumption that they have a Maxwellian velocity distribution and can be adequately described by moment equations. This

has been shown previously to be incorrect,[6] so the results obtained in this theory will be qualitatively correct at best. On account of the relatively low frequency of the waves and the high collision frequency of the electrons, both ω and Z_i may be neglected relative to the collision frequency, ν_-. Then the conservation equations corresponding to (5) and (6) for the ions are

$$ikV_-n + ikNv = 0 \tag{10}$$

$$imNkV_-v = -qNe - mN\nu_-v - ikTn. \tag{11}$$

Since $V_- = -\frac{qE}{m\nu_-}$, Eqs. 10 and 11 give

$$\frac{e}{E} = -\left[1 + i\frac{kT}{qE}\left(1 + \frac{V_-^2 m}{T}\right)\right]\frac{n}{N}.$$

Since $V_-^2 \ll \frac{T}{m}$,

$$\frac{e}{E} = -\left[1 + i\frac{kT}{qE}\right]\frac{n}{N}. \tag{12}$$

Equation 12 is one of the two equations relating n, e, and z_i that is needed to obtain a dispersion relation. Now, for small-amplitude waves, assume that

$$z_i = Z_i'\delta T \tag{13}$$

is valid, where

$$Z_i' = \left.\frac{\partial Z_i}{\partial T}\right]_{T_o},$$

with δT the time-variant part of the electron temperature, and T_o the electron equilibrium temperature. A relationship has been derived relating the axial electric field to the electron temperature which, after being linearized, is[2]

$$\frac{\partial(\delta T)}{\partial z} = a_1(\delta T) - b_1 e, \tag{14}$$

where

$$a_1 = \frac{16T_o}{3\pi qE\ell_-^2}\left[2k^* + T_o\frac{\partial k^*}{\partial T}\right]$$

$$b_1 = \left[\frac{3}{2} + \frac{16T_o k^*}{3\pi q E \ell_-}\right] q.$$

Here, ℓ_- is the electron mean-free path, and k^* is the fractional electron energy loss per electron-neutral collision. Combining (13) and (14) gives

$$z_i = \frac{Z_i' b_1}{a_1 - ik} e. \tag{15}$$

Dispersion Relation

Combining (7), (12), and (15) gives the dispersion relation

$$\frac{-\omega'}{1 + ik\left(\frac{T_o}{qE}\right)} = \frac{kV}{1 + \frac{Z_i}{\nu_+} - \frac{i\omega'}{\nu_+}} + \left[i\frac{-kV}{(-i\omega' + \nu_+ + Z_i)}\right]\frac{Z_i' b_1 E}{(a_1 - ik)}. \tag{16}$$

It can be shown that for the experimental regime under consideration $b_1 \approx \frac{3}{2} q$. Now define

$$\omega_s = \frac{3}{2} Z_i' T_o.$$

Then define the two dimensionless variables

$$f' = \omega'/\omega_s$$

$$\zeta = k\left(\frac{T_o}{qE}\right).$$

Then (16) can be written

$$\frac{-f'}{1 + i\zeta} = \frac{V\zeta}{\omega_s L\left[1 - i\frac{\omega_s}{\nu_+} f' + \frac{Z_i}{\nu_+}\right]} + \left[i\frac{-V\zeta}{\omega_s L\left(-if' + \frac{\nu_+}{\omega_s} + \frac{Z_i}{\omega_s}\right)}\right] \cdot \frac{1}{a_1 L - i\zeta}, \tag{17}$$

where $L = \frac{T_o}{qE}$.

In order to proceed further, we must put in realistic values for the quantities appearing in (17). The plasma under consideration for this special discussion is an Argon plasma, in a low-pressure glow discharge. I find experimentally that

$$E \approx 1 \text{ V/cm} \qquad T_o \approx 6.5 \text{ eV},$$

and therefore

$$L \approx 6.5 \text{ cm.}$$

Assume $k^* \approx \frac{2m}{M} = 2.8 \times 10^{-5}$. Now, keeping the pressure dependence explicit in the other quantities, we obtain

$$\ell_- \approx \frac{.08}{P} \text{ cm-Torr} \quad \text{for 6-eV electrons in A,}$$

and therefore

$$a_1 \approx \frac{90}{\text{cm}} \frac{P^2}{\text{Torr}^2}$$

$$b_1 = \frac{3}{2} q.$$

Under the assumption that T_o is independent of P,

$$Z_i' \approx \frac{2 \times 10^4}{\text{eV-sec}},$$

and therefore

$$\omega_s \approx 1.3 \times 10^5 \text{ sec}^{-1}.$$

Here the value of Z_i' has been chosen to fit theory with experiment. The computation of Z_i' is fraught with uncertainties, especially at low pressures, since the electrons are not Maxwellian. This is a degree of freedom in the theory which can probably be eliminated by careful computation. Work on this problem is in progress.

For Argon,

$$\nu_+ \approx \frac{.3 \times 10^8 \, P}{\text{sec-Torr}}$$

$$V \approx \mu_+ E \approx \frac{760}{P} \frac{\text{cm}}{\text{sec}} - \text{Torr}$$

for E = 1 V/cm.

Substituting these numbers back into (17) and keeping the P dependence explicit, we obtain

$$i \frac{K_1}{P} f'^2 - \left[1 + \frac{K_1 K_4}{P^2} + iK_1 H\right] f' + \left[\left(1 + \frac{K_1 K_4}{P^2}\right) H - \frac{K_2}{P}(1+i\zeta) + i \frac{K_1 K_2}{P^2} \zeta H\right] = 0. \qquad (18)$$

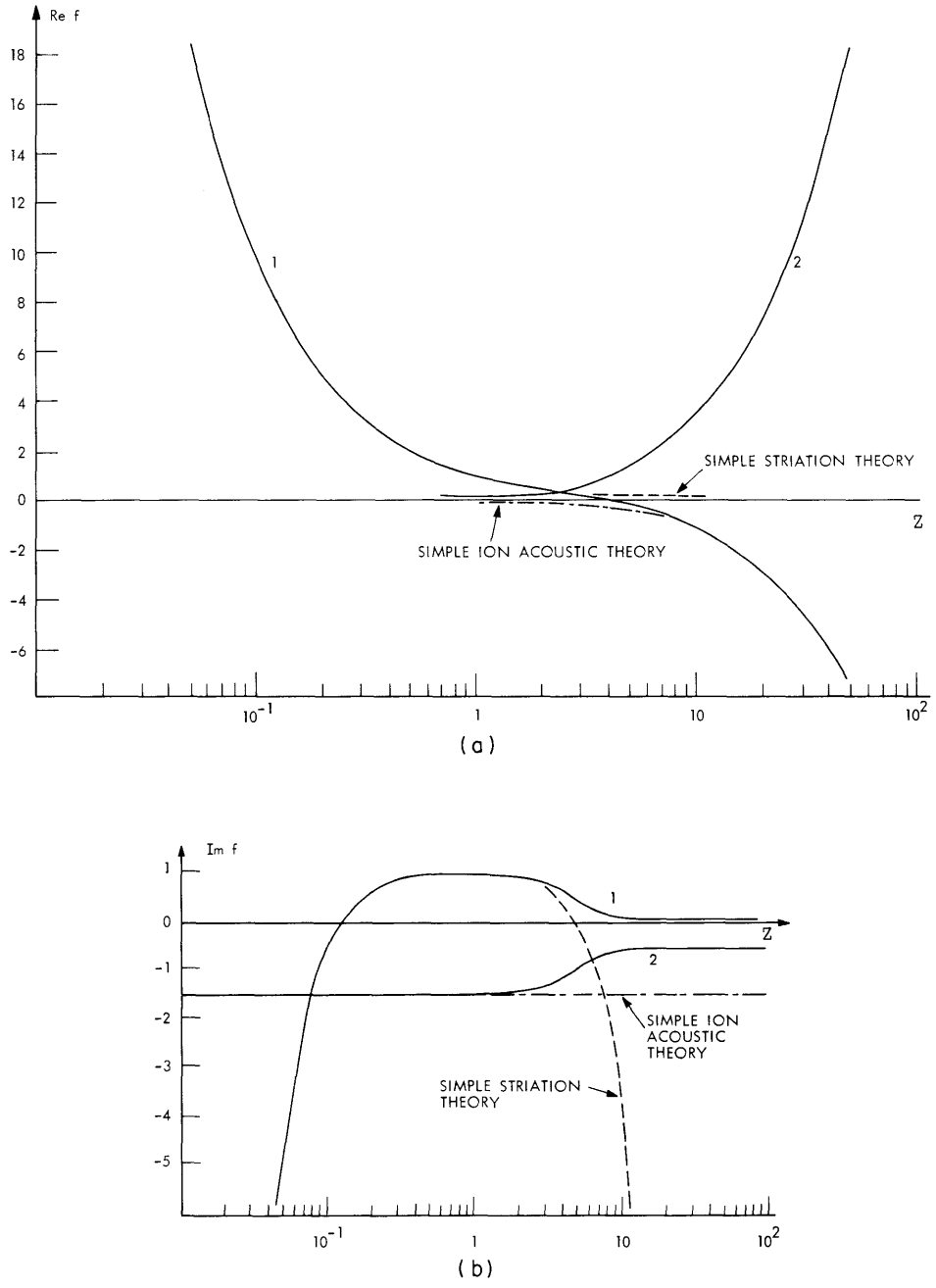

Fig. VI-4. Two solutions to the dispersion relation: (a) Real part of f vs ζ. (b) Imaginary part of f vs ζ. ζ is assumed to be real. Also shown is the dispersion relation for simple ion acoustic waves ($Z_i'=0$) and the dispersion relation for simple striations ($\omega \ll \nu_+$).

Here

$$H = \frac{1 + i\zeta}{\zeta + iK_2P^2}$$

$$\frac{K_1}{P} = \frac{\omega_s}{\nu_+} = \frac{.75 \times 10^{-2}}{P}$$

$$\frac{K_2}{P} = \frac{\mu_+ E}{\omega_s L} = \frac{.52 \times 10^{-3}}{P}$$

$$K_3P^2 = a_1L = 585\ P^2$$

$$\frac{K_4}{P} = \frac{Z_i}{\omega_s} \approx \frac{3.9 \times 10^{-3}}{P},$$

with P in Torr. Equation 18 has been solved for f' vs ζ, and then the transformation to the laboratory frame has been made to give f vs ζ. Figure VI-4 shows the two roots for P = 0.005 Torr; ζ is assumed real, and the real and imaginary parts of f are plotted. Root 2 is the ion acoustic mode that propagates from anode to cathode. For this wave, $\omega_{real} = \left[\sqrt{\frac{T}{M}} + V\right] k$, thereby giving the usual velocity for an ion acoustic wave in a drifting medium.

In the region where ζ is greater than approximately 7, the behavior of the other root is like that of the ion acoustic wave in the other direction, with

$$\omega_{real} = -\left[\sqrt{\frac{T}{M}} - V\right] k.$$

For small values of ζ, the wave follows the dispersion relation predicted by Pekarek's theory, which says that if $k \gg a_1$, $\omega_{real} \approx \frac{\omega_s}{kL}$, or $f \approx \frac{1}{\zeta}$.

The imaginary parts of roots 1 and 2, shown in Fig. VI-4b, go to the simple striation and ion acoustic theory limits for ζ small. For δ large, they are modified, because of coupling between the two modes. Note that this theory predicts Im f > 0 for root 1, which implies growth in time. In fact, this is not observed. Theory and experiment agree qualitatively, however, because the region $0.5 < \zeta < 3$, where Im f is a maximum, is the region in which relatively undamped waves can be excited experimentally.

Summary

A theory has been presented that shows that ion acoustic waves and striations

can be derived from a single theory. The agreement between theory and experiment is only qualitative, however, because of the approximation of using moment equations for the electrons. A more detailed analysis with the Boltzmann equation used to describe the electron motion is in progress.

D. W. Swain

References

1. N. L. Oleson and A. W. Cooper, Advances in Electronic and Electron Physics 24, 155 (1968).
2. L. Pekarek and V. Krejci, Czech. J. Phys. B11, 729 (1961); B12, 296 (1962); B12, 450 (1962).
3. H. Tanaca et al., Phys. Rev. 161, 94 (1967).
4. G. M. Sessler and G. A. Pearson, Phys. Rev. 162, 108 (1967).
5. I. Alexeff and W. D. Jones, Phys. Fluids 9, 1871 (1966).
6. D. W. Swain, Quarterly Progress Report No. 91, Research Laboratory of Electronics, M.I.T., October 15, 1968, p. 82.

4. NONLINEAR INSTABILITIES IN MULTICOMPONENT PLASMAS

During the past quarter, we have been investigating the nonlinear stability of thermal plasma coexisting with a low density of energetic electrons. If a weak magnetic field is present, electron plasma waves are linearly unstable, but the growth rates are very small. Since such a plasma obviously has a great deal of free energy, it seems reasonable to assume that the plasma is also nonlinearly unstable. We find this to be the case. Two plasma waves at $(\omega, \underline{k})$, $(\omega', \underline{k}')$ can interact with an energetic particle having velocity $\underline{v}$, as long as

$$\omega \pm \omega' - (k' \pm k')_z v_z - n\omega_c = 0. \tag{1}$$

For such an interaction, the nonlinear growth rate of each wave may be calculated. If the negative sign is chosen above, one wave grows and the other damps, while if the positive sign is chosen, both waves either grow or damp. To find the total nonlinear growth rate for a wave at ω, one must sum the growth rate for each interaction over all waves with which the wave at ω can interact, over all perpendicular particle velocities, over all cyclotron harmonics, and over plus and minus ω'.[1]

The details of the calculation will be given elsewhere.[2] The final result, however, is that both waves tend to grow, and that the nonlinear growth rate may dominate the linear growth rate for very small wave energies. For example, for typical parameters of the solar corona at 10 solar radii, $n_o \approx 10^4/\text{cm}^3$, $B = 10^{-2}$ G. If for the energetic

particles, we choose $\frac{n_n}{n_o} \approx \frac{1}{100}$ and E = 3 keV, the energy density of energetic particles will be approximately one-tenth of the magnetic energy density. Then the linear growth rates are typically $\gamma \sim 10^4 \omega_{pe}$, and the nonlinear growth rates dominate when

$$\frac{E_{wave}}{E_{hot\ particles}} \sim 10^{-5}.$$

W. M. Manheimer

References

1. W. M. Manheimer (to be published in Phys. Fluids).
2. W. M. Manheimer (to be submitted for publication).

5. COLLISIONAL CYCLOTRON INSTABILITY IN A XENON PLASMA

Introduction

Some preliminary results obtained on a study of the collisional cyclotronic instability in a weakly ionized plasma of a xenon glow arc discharge are reported here. Twiss[1] and Bekefi, Hirshfield, and Brown[2] have studied theoretically the linear theory of the collisional cyclotron instability and have shown that (as in a maser) there are two criteria for its appearance.

1. A nonthermal distribution f of the electron velocity v with an overpopulation of energetic electrons

$$\frac{\partial f(v)}{\partial v} > 0$$

in some range of electron velocities.

2. A higher lifetime, or a smaller probability of spontaneous emission $\eta_\omega(v)$, for the upper velocities

$$\frac{\partial}{\partial v}[v\eta_\omega(v)] < 0$$

in the same range of electron velocities as in criterion 1.

The anomalous radiation that is the result of this instability has been widely investigated experimentally by Tanaka, Mitani, and Coccoli,[3] Bekefi,[4] and Coccoli.[5] On a certain number of points the experimental results agree fairly well with the theory.[4,6] The radiation, 20 dB above the thermal noise, is observed only in the vicinity of

electron-cyclotron frequency, and for gases with pronounced Ramsauer effects, such as Xe, Kr, and Ar; the width of the anomalous cyclotron radiation peak is much less than the frequency of electron-atom elastic collisions; the radiation is detected only in the cathode part of the investigated discharge tube where an electron velocity distribution is expected with a peak in the range of velocity in which the collision cross section is rapidly increasing. Some points are still unexplained, however.

1. As has been reported,[7, 8, 9] the emission appears in pulses that are related in phase to a low-frequency oscillation that is present in the tube. A problem that arises is the determination of the nature of this low-frequency oscillation and its influence on the different parameters of the plasma and on the radiation. In resolving this problem, we hope to give an explanation of the fast saturation of the experimentally observed amplification[10] (or negative absorption).

2. Although this instability has been theoretically investigated in the case of a tenuous medium (no collective effects), the observations[11] were made for a broad range of electron densities, where the plasma frequency ω_p is of the same order as the cyclotron frequency ω_B. The problem is to understand the influence of the density on the propagation of the anomalous radiation and to investigate the different modes in which collective effects can appear.

3. Except in cases for which probes are used, the methods used to pick up the radiation (cavity or waveguide) do not permit good localization of the source of the radiation and accurate determination of its polarization.

For these reasons, we have adopted the experimental design described here.

Experimental Design

In order to be able to act upon and control the electron velocity distribution function in the cathode region of the discharge, a ring electrode (in this report called a "grid") is placed between the positive column and the negative glow of a Xenon plasma tube (Fig. VI-5). Under our experimental conditions, the discharge has the characteristics of a low-voltage arc (the potential drop V_d in the tube is $\approx$10 V and is almost constant for discharge currents in the range 50 mA $\leq I_d \leq$ 600 mA) with random anodic sheath fluctuations, $\Delta V \sim 1V$. To have accurate measurements of the location and polarization of the radiation, we monitor it through a small circumferential coupling gap (of variable width from 0 to 1 cm) in the internal cylinder of a coaxial cavity that fits around the tube. The cavity mode used is the TE_{011} (resonant frequency f_o = 5.5 GHz), having only an azimuthal electric field corresponding to the polarization of the extraordinary wave in the plasma. Furthermore, the radiation can be picked up by a strip line (as shown in Fig. VI-5) consisting of two metal curved strips around the tube. Also, visible light emanating from the circumferential gap is received through a light pipe. The block diagram of the entire experimental design is shown in Fig. VI-6.

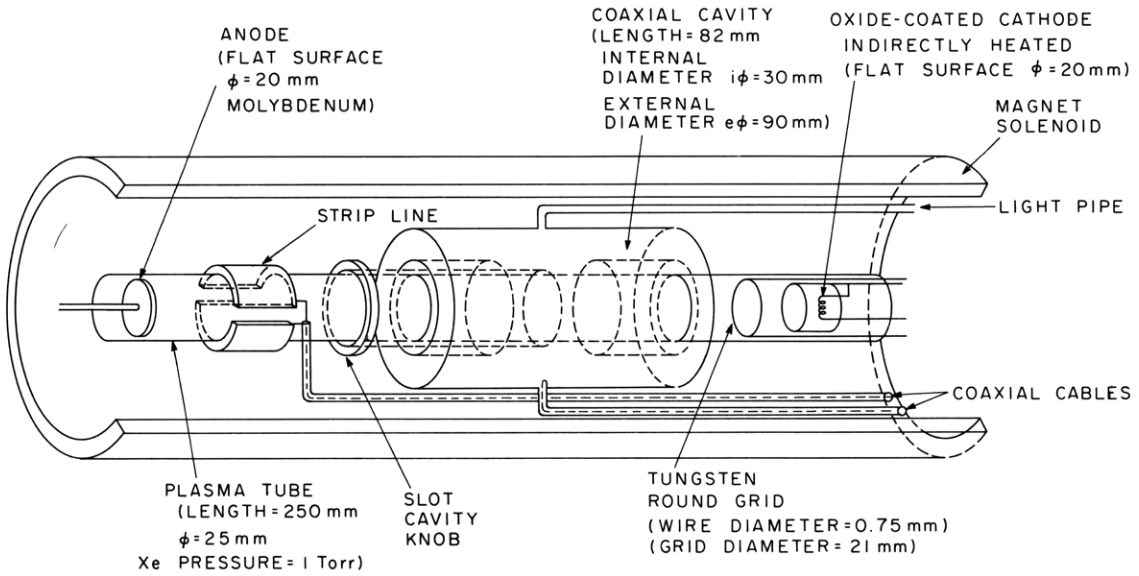

Fig. VI-5. Experimental apparatus.

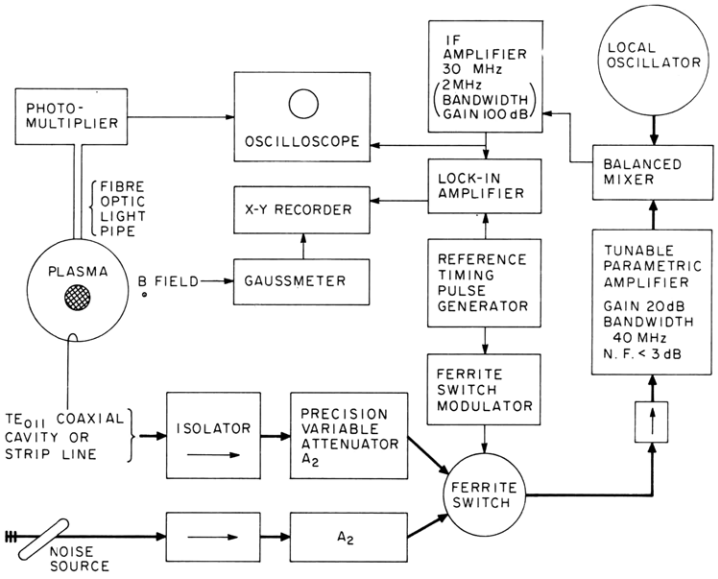

Fig. VI-6. Diagram of the experiment.

Experimental Results and Discussion

a. Measurements of n_e and T_e in the Case of Equilibrium (No Voltage Applied to the Ring and No Magnetic Field)

The coaxial cavity is also used to obtain an estimate of the electron density and temperature as a function of current. The determination of density was made with the maximum opening of the gap (1 cm) and can be only approximated, because of the difficulty in determining the configuration of the field inside the plasma. The first-order relation between the shift, Δf, and the plasma frequency

$$\frac{\Delta f}{f_o} = -\frac{1}{2}\,\frac{1}{\omega^2 + \nu_m^2}\,\frac{\int \omega_p^2 |\vec{E}_o|^2}{\int |\vec{E}_o|^2\, dV}$$

can be only approximate because it is difficult to know the field $\vec{E}_o(\vec{r})$ exactly. Experimentally, the determination of small frequency shifts (only a few MHz because of a small loading of the cavity by the plasma) leads to large errors. Indeed, for small density ($I_d < 100$ mA) the frequency shift of the coaxial cavity was calibrated by comparison with that of a different cylindrical cavity (in the TM_{020} mode, $f_o = 4420$). Under the assumption of a collision-limited diffusion leading to the radial distribution of electron density $n = n_o J_o(2.4r/R)$, where n_o is the axial density, and R the tube radius, the results are in fair agreement with the simple formula giving the current density

$J = n e \mu E$, where E is the mean field in the tube, and μ the electron mobility. The density n is nearly constant along the tube and shows a linear dependence upon the current I from 1.5 to 9.5×10^{11} e-cm^{-3} for 50-500 mA. These results correspond to a plasma frequency $\omega_p \approx \omega_B$ for the experimental conditions described here.

The determination of temperature by measurements of power emitted by the cavity-plasma system requires measurement of the VSWR of this system according to the formula[13]

$$T_R - T_o = \frac{a_s/a_c}{\left(1 - \frac{\sigma_1}{\sigma_2}\right)(1-|\Gamma|^2)} (T_s - T_o).$$

This gives the difference between the plasma radiation temperature T_R and the room temperature T_o as a function of the VSWR, σ, of the plasma cavity system termination (the indexes 1 and 2 meaning the plasma "off" or "on") and $|\Gamma|^2$, the power reflection coefficient with the plasma on. The parameters a_s and a_c are the absorption of attenuators in front of the noise standard and the plasma when balance between the two is achieved. In the same range of current as discussed above, the radiation temperature varies from 1.4×10^4°K to 1.7×10^4°K.

b. Location of the Anomalous Radiation

To localize the source of the radiation, the size of the cavity gap opening on the plasma tube is reduced to 1 mm. While passing through the resonance by varying the magnetic field, the output power of the comparison radiometer is displayed on the y trace of the x-y recorder, with the x trace related to the position along the tube. The envelope of such data is shown in Fig. VI-7, which shows that the anomalous radiation is emitted only in that part of the discharge where the plasma parameters are strongly modified.

The same results are obtained in the cathode region with the strip line. Nevertheless, in the last case we pick up along the whole positive column radiation of lesser amplitude that shows a stationary wave pattern and is in phase with the oscillation of the light emitted from the cathode region (and not with the light emitted in the positive column). We deduce from this observation that the strip line picks up a wave, excited by the collisional instability near the cathode, which propagates along the tube.

c. Spectrum and Variation in Time of the Collisional Instability

Apart from a difference in the width of the spectrum, the radiation picked up by the strip line and by the cavity have the same behavior when placed in the cathode region at the point of maximum intensity. Data on the intensity of the high-frequency radiation

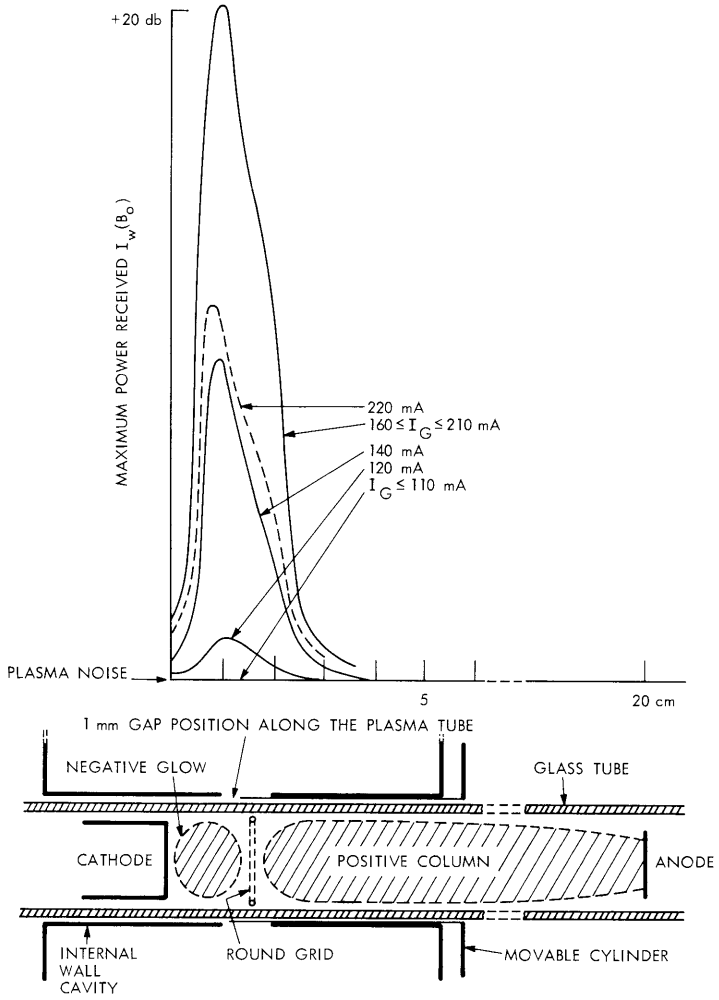

Fig. VI-7. Location of the anomalous radiation received by the cavity. Current discharge, I_d = 200 mA.

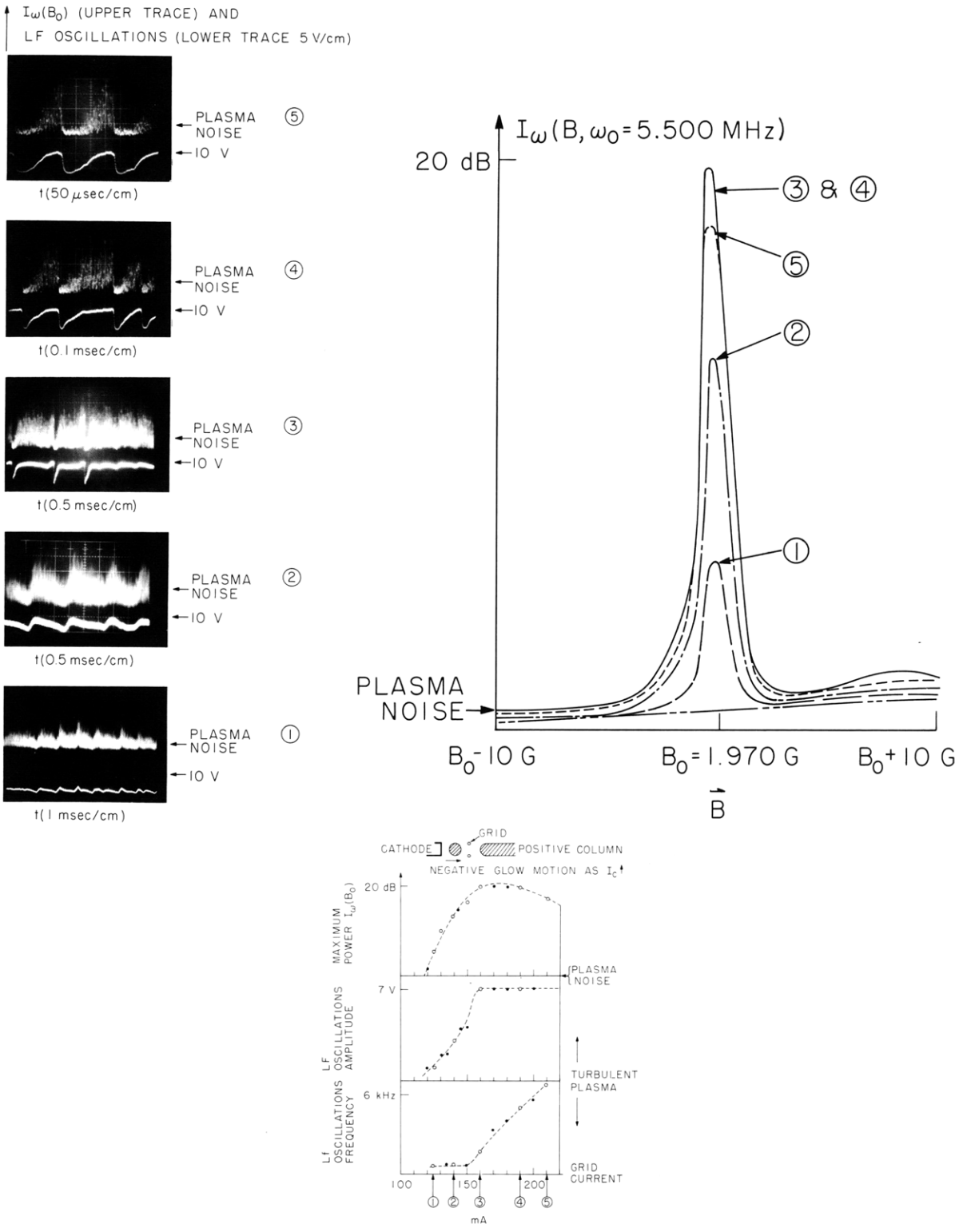

Fig. VI-8. Anomalous cyclotron emission picked up by the strip line (current discharge 200 mA, voltage discharge 10 V).

as a function of B and variation in time compared with the oscillation are reported in Fig. VI-8. The principal features are the following.

1. An extremely small width corresponding at the lower limit to that imposed by the nonuniformity of the magnetic field and the bandwidth of the IF amplifier (2 MHz).

2. A variation in time of the radiation with a definite phase relation to the low-frequency oscillation. The two are in phase.

3. For a constant anode current of 200 mA, with increasing grid potential V_G and grid current I_G, three different regimes may be seen

$$V_F = -4v < V_G < +2 \text{ V}, \quad 0 < I_G < 110 \text{ mA}, \tag{1}$$

characterized by random and low-amplitude low-frequency oscillations corresponding to the fluctuations in the positive column. No anomalous radiation is emitted.

$$+2v < V_G < +11 \text{ V}, \quad 110 < I_G < 160 \text{ mA}, \tag{2}$$

with continuous increase in the low-frequency oscillation corresponding to an increase in the high-frequency anomalous cyclotron radiation.

$$V_{G_{max}} = +11 \text{ V}, \quad 160 < I_G < 210 \text{ mA}. \tag{3}$$

(We are limited in this range of current by a turbulent state that appears when we draw too much current ($I_G > 210$ mA) in the cathode region.) The amplitude of the low-frequency oscillation is constant, and the frequency increases continuously. The high-frequency radiation amplitude remains stationary and decreases when turbulence appears.

4. With increasing current the negative glow is displaced slightly in the cathode-grid direction.

Tanaka and Takayama[11] have reported the same interdependence of the intensity of high-frequency radiation, and the amplitude and frequency of low-frequency oscillation with changing current. Nevertheless, under their experimental conditions, the over-all current dependence of these quantities is the inverse of that reported here. For example, in their case the amplitude of low-frequency oscillation decreased with increasing discharge current. At this time, no valid explanation for the phenomena has been found.

Conclusion and Program for Further Research

This preliminary experiment seems to show that it is difficult to act independently on the velocity distribution function without modifying the plasma parameters (electron density, plasma potential) and the stability. With fast pulsed techniques, however, we

hope to study the anomalous radiation in the absence of the oscillations present in the steady-state discharge. Under the experimental conditions described here, it is difficult to find a coherent model for the creation of the peak in f(v). Further experiments will be made in order to confirm the existence of the peak in f(v), which is required by the linear theory of collisional instability.

C. Oddou

References

1. R. Q. Twiss, Australian J. Phys. 11, 564 (1958).
2. G. Bekefi, J. L. Hirshfield, and S. C. Brown, Phys. Fluids 4, 173 (1961); Phys. Rev. 122, 1037 (1961).
3. S. Tanaka, K. Mitani, and H. Kubo, "Experiments on the Negative Radiation Temperature at Cyclotron Resonance in Cold Plasma," Nagoya University, Institute of Plasma Physics, Report IPPJ 6, February 1963.
4. G. Bekefi, Radiation Processes in Plasmas (John Wiley and Sons, Inc., New York, 1966).
5. J. D. Coccoli, Quarterly Progress Report No. 72, Research Laboratory of Electronics, M.I.T., January 15, 1964, p. 102.
6. C. Oddou, 3^{d} Cycle Thesis, University of Paris, January 1966.
7. J. D. Coccoli, Quarterly Progress Report No. 73, Research Laboratory of Electronics, M.I.T., April 15, 1964, p. 35.
8. S. Tanaka, "Anomalous Pulsed Microwave Emission of Cyclotron Frequency in Partially Ionized Plasma," J. Phys. Soc. Japan 21, 10 (1966).
9. C. Oddou and B. Dulieu, LEGI Internal-Report No. 62, June 1967.
10. K. Mitani, S. Tanaka, and Y. Terumichi, VII^{e} ICPIG, Belgrade, 1965.
11. S. Tanaka, K. Takayama, J. Phys. Soc. Japan 21, 2372-2380 (1966).
12. J. C. Ingraham and S. C. Brown, "Plasma Diagnostics," Technical Report 454, Research Laboratory of Electronics, M.I.T., Cambridge, Massachusetts, October 3, 1966.
13. E. F. Labuda and E. I. Gordon, J. Appl. Phys. 35, 1647 (1964).

6. INSTABILITIES DRIVEN BY HOT ELECTRONS IN A MAGNETIC MIRROR

Introduction

Our previous reports have been concerned with the experimental study of a high-frequency instability present in our mirror-confined hot-electron plasma. This study has revealed that the frequency of the instability is essentially equal to that of a resonance of the microwave cavity in which the plasma is generated.[1] In this experiment the static magnetic field is highly nonuniform over the extent of the plasma.[2] It is observed, however, that the occurrence of the instability requires that the instability

frequency be close to the local electron-cyclotron frequency in the region where the electric field of the resonant mode is strongest.[3] Thus the instability does appear to arise from a coupling between the electric field and the cyclotron motion of the electrons. This motion is not, however, the simple helical path of an electron in a uniform field, but rather the more complicated trajectory of a charged particle confined in a mirror magnetic field. Two important aspects of this motion are that first, a given electron is only instantaneously resonant with the wave frequency as it passes through the location with the proper cyclotron frequency and second, since the electron is confined by the magnetic field, it will periodically pass through this location. Both of these aspects, along with the experimental observation that the presence of the cavity greatly affects the characteristics of the instability, cast doubt on our original plan to identify the instability with that of existing infinite plasma theories.[4]

A formal method for including the effect of the cavity has been previously presented by Bers.[5] In this report we present a simple model that attempts to account for the effects that the complicated particle trajectories that are due to the nonuniform magnetic field introduce into the interaction between the plasma and the RF electric field.

Theoretical Model and Its Motivation

At the time of the instability it is observed experimentally that the plasma is so tenuous that the resonant frequency of the plasma-cavity system is only slightly changed from that of the empty cavity. This would indicate that the majority of the RF energy resides in the electromagnetic fields rather than in the plasma medium and that these fields are only slightly altered from their empty cavity form. Thus the main effect arising from the presence of the electrons is their absorption (or generation) of power from the RF electric field of the high-Q cavity mode. Perturbation theory would then predict that the frequency of the mode (assumed to have an $e^{j\omega t}$ time dependence) would become complex, with the imaginary part of the frequency (assumed small) satisfying the relation

$$2\omega_i\langle W\rangle = \langle P_M\rangle + \langle P_W\rangle, \tag{1}$$

where $\langle W\rangle$ is the time average energy stored in the fields, $\langle P_M\rangle$ the time-average power dissipated in the medium, and $\langle P_W\rangle$ the power dissipated in the cavity walls. In the following calculations we are concerned with the determination of $\langle P_M\rangle$, with particular interest in those conditions predicting growth of the RF fields ($\langle P_M\rangle + \langle P_W\rangle$, and hence ω_i less than zero).

The system that we consider is shown in Fig. VI-9. The static axial magnetic field is assumed to vary with z according to the expression

$$B_z = B_o\left(1 + \frac{z^2}{L^2}\right). \tag{2}$$

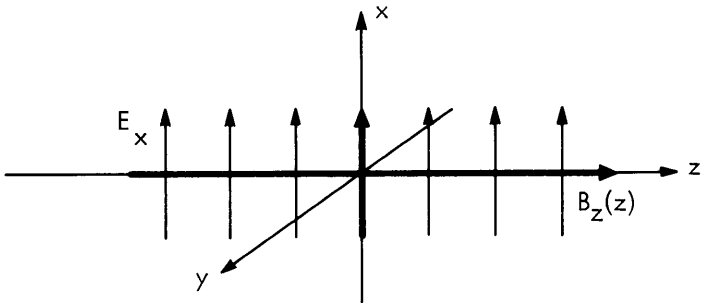

Fig. VI-9. Geometry for the interaction of electrons with an RF electric field and a static nonuniform magnetic field.

Only electrons whose guiding centers are on the z axis will be considered, although off-axis electrons could be included approximately by interpreting z as the dimension along a field line. The RF electric field is taken to be uniform in the x direction, and independent of the z coordinate, while the RF magnetic fields are ignored. These assumptions greatly simplify the calculations, but still reflect the salient features of the experimental observations. To a high degree of approximation, the measured axial magnetic field is parabolic. The observed instability radiation appears in the TE_{231} cylindrical cavity mode which exhibits an electric field purely transverse to the z axis. Transverse variation in the amplitude of this field should be unimportant for electrons whose Larmor orbit is sufficiently small. Likewise, the cosine variation of the electric field along the axis of the cavity should be unimportant for electrons that do not move too far from the midplane of the cavity. Neglect of the RF magnetic fields appears justified, as long as the velocity of the electrons is small compared with the velocity of light, so that the resulting forces are small in comparison with those of the electric field.

Theory

We begin with the linearized Vlasov equation, which predicts that the first-order distribution function for the electrons is given by

$$f_1(\bar{r}, \bar{v}, t) = \frac{e}{m} \int_{-\infty}^{t} \left(\bar{E}_1 \cdot \frac{\partial f_o}{\partial \bar{v}} \right)' dt', \tag{3}$$

where $\bar{E}_1$ is the first-order electric field, and f_o is the unperturbed electron velocity distribution which must satisfy the zero-order Vlasov equation. The prime indicates that the integral is to be evaluated along the unperturbed orbits of the electrons. We take the electric field to be of the form

$$\bar{E}_1 = E_o e^{j\omega t} \bar{i}_x,$$

where E_o is a constant, and ω is assumed to have a small negative imaginary part. (We have also considered the case of a circularly polarized field; the results are very similar to those quoted below.)

For the zero-order orbits we take the solution of the equation of motion of an electron in the parabolic magnetic field, subject to the adiabatic approximation. This solution, for an electron which at time $t' = t$ is located at $z' = z$ with a velocity perpendicular to the magnetic field of $v'_\perp(\cos\phi'\bar{i}_x + \sin\phi'\bar{i}_y) = v_\perp(\cos\phi\bar{i}_x + \sin\phi\bar{i}_y)$, is

$$z' = z_o \cos\left[\cos^{-1}\left(\frac{z}{z_o}\right) - \omega_m(t-t')\right] \tag{4}$$

$$v'_\perp = \frac{v_\perp}{\left(1+\frac{z^2}{L^2}\right)^{1/2}}\left\{1 + \frac{z_o^2}{L^2}\cos^2\left[\cos^{-1}\left(\frac{z}{z_o}\right) - \omega_m(t-t')\right]\right\}^{1/2} \tag{5}$$

$$\phi' = \phi - \bar{\omega}_c(t-t') + \frac{\omega_{co} z_o^2}{4L^2\omega_m}\left\{\sin 2\left[\cos^{-1}\left(\frac{z}{z_o}\right) - \omega_m(t-t')\right] - \sin 2\left[\cos^{-1}\left(\frac{z}{z_o}\right)\right]\right\}, \tag{6}$$

where L is the scale length of the magnetic field (see Eq. 2), $z_o = \frac{v_{110}L}{v_{\perp 0}}$ is the axial reflection point for an electron whose midplane velocity components along and across the magnetic field are, respectively, v_{110} and $v_{\perp 0}$, $\omega_m = \frac{v_{\perp 0}}{L}$ is the "mirror" frequency of the electron, ω_{co} is the midplane cyclotron frequency eB_o/m, and $\bar{\omega}_c = \omega_{co}\left(1+\frac{z_o^2}{2L^2}\right)$ is a quantity that may be interpreted physically as the average of the cyclotron frequencies along the orbit of the electron. The zero-order electron distribution function can be expressed as an arbitrary function of the constants of the motion ($E = \frac{m}{2}\left(v_{110}^2 + v_{\perp 0}^2\right)$ and the magnetic moment $\mu = \frac{mv_{\perp 0}}{2B_o}$, an adiabatic invariant), subject to the constraint that it represents confined electrons. Defining $\tau = t - t'$ and evaluating the integral of Eq. 3 along the unperturbed orbits, we find

$$f_1 = \frac{e}{m}\int_0^\infty \left(\bar{E}_1 \cdot \frac{\partial f_o}{\partial v}\right)' d\tau, \tag{7}$$

where

$$\left(\bar{E}_1 \cdot \frac{\partial f_o}{2v}\right)' = E_o\, e^{j\omega(t-\tau)}\, W \cos\left[\phi - N\sin 2\xi - \bar{\omega}_c\tau + N\sin 2(\xi - \omega_m\tau)\right], \tag{8}$$

with

$$N = \frac{\omega_{co} z_o^2}{4L^2 \omega_m} \tag{9}$$

$$\xi = \cos^{-1}\left(\frac{z}{z_o}\right) \tag{10}$$

$$W = \frac{(2e)^{1/2}\,\mu^{1/2}}{\left[\bar{\omega}_c + 2\omega_m N \cos 2(\xi - \omega_m \tau)\right]^{1/2}} \frac{\partial f_o}{\partial \mu} + (2/e)^{1/2}\, m\mu^{1/2}$$

$$\cdot \left[\bar{\omega}_c + 2\omega_m N \cos 2(\xi - \omega_m \tau)\right]^{1/2} \frac{\partial f_o}{\partial E}. \tag{11}$$

It should be remembered that on the τ integration z, ϕ, and z_o are constants. Making the substitution

$$y = 2(\xi - \omega_m \tau), \tag{12}$$

using the identity

$$e^{\pm jA \sin y} = \sum_{n=-\infty}^{\infty} e^{\pm jny}\, J_n(A), \tag{13}$$

and, subject to the approximation that for W,

$$\frac{2\omega_m N}{\bar{\omega}_c} = \frac{z_o^2}{2L^2} \frac{1}{\left(1 + \frac{1}{2}\frac{z_o^2}{L^2}\right)} \ll 1, \tag{14}$$

we find

$$f_1 = \frac{e}{m} E_o\, e^{j\omega t}\, I \left[\left(\frac{e}{2}\right)^{1/2} \frac{\mu^{1/2}}{\bar{\omega}_c^{1/2}} \frac{\partial f_o}{\partial \mu} + \left(\frac{2}{e}\right)^{1/2} \frac{m\mu^{1/2}\bar{\omega}_c^{1/2}}{2} \frac{\partial f_o}{\partial E}\right], \tag{15}$$

where

$$I = \sum_{n=-\infty}^{\infty} \frac{J_n(N)}{j} \left[\frac{e^{j(\phi - N \sin 2\xi + 2n\xi)}}{\omega + \bar{\omega}_c + 2n\omega_m} + \frac{e^{-j(\phi - N \sin 2\xi + 2n\xi)}}{\omega - \bar{\omega}_c - 2n\omega_m}\right]. \tag{16}$$

The approximation, which allows us to neglect the τ variation of W, requires that we consider only electrons whose maximum penetration into the mirror is small compared with the "doubling" distance of the magnetic field. In essence, the approximation reflects the fact that for these electrons we can neglect the small variation in the magnitude of its transverse velocity as it travels along its orbit (see Eq. 8). A similar term appearing in the phase of the transverse velocity (Eq. 6) may not be neglected, since accumulated phase differences for small changes in z_o^2/L^2 may be quite large.

We are interested in obtaining the time-average power absorbed by the electrons in the presence of the electric field. This power per unit transverse area is given by

$$\langle P_M \rangle = \frac{1}{2} \operatorname{Re} \int_{-z_{max}}^{+z_{max}} dz\, E_o^* e^{-j\omega t} J_x, \tag{17}$$

where z_{max} is the location of the mirror peak, and

$$J_x = -e \int v_\perp \cos\phi\, f_1\, d^3v \tag{18}$$

is the x component of the first-order current density induced by the electric field. Noting that the volume element of velocity space can be written

$$d^3v = v_\perp d\phi dv_\perp dv_{11} = \left(\frac{2}{m}\right)^{1/2} \frac{B}{2m} (E-B\mu)^{-1/2}\, d\phi dE d\mu, \tag{19}$$

where B is given by Eq. 2, we find, after performing the ϕ integration and again using the identity of Eq. 13, that

$$J_x(z) = -\frac{e^2}{m} E_o e^{j\omega t} \pi \left(\frac{2}{e}\right)^{1/2} \frac{B}{2m} \int_0^\infty dE \int_{E/B_{max}}^{E/B} d\mu\, \frac{\bar{\omega}_c^{1/2} \mu I'}{\left(\frac{E}{B}-\mu\right)^{1/2}} \left(\frac{e}{m} \frac{1}{\bar{\omega}_c} \frac{\partial f_o}{\partial \mu} + \frac{\partial f_o}{\partial E}\right), \tag{20}$$

where

$$I' = \sum_{n=-\infty}^{\infty} \sum_{\ell=-\infty}^{\infty} \left\{ \frac{J_n(N)\, J_\ell(N)}{j} \left[\frac{e^{j2(n-\ell)\xi}}{\omega + \bar{\omega}_c + 2n\omega_m} + \frac{e^{-j2(n-\ell)\xi}}{\omega - \bar{\omega}_c - 2n\omega_m} \right] \right\}. \tag{21}$$

In terms of the integration variables, we have

$$\bar{\omega}_c = \frac{\omega_{co}}{2} \left(1 + \frac{E}{B_o \mu}\right) \tag{22}$$

$$\omega_m = \left(\frac{2B_o}{m}\right)^{1/2} \frac{\mu^{1/2}}{L} \tag{23}$$

$$N = \frac{\omega_{co} L}{4\left(\frac{2B_o}{m}\right)^{1/2}} \frac{(E/B_o\mu - 1)}{\mu^{1/2}} \tag{24}$$

$$\xi = \cos^{-1}\left[\frac{z}{L\left(\frac{E}{B_o\mu} - 1\right)^{1/2}}\right]. \tag{25}$$

The limits of integration on μ reflect the fact that the electrons under consideration must indeed be those confined by the magnetic mirror. In particular, at a given location within the magnetic field (as implied by the dependence of B upon z), an electron with energy E must have at least the minimum magnetic moment, or else its reflection point would exceed the mirror peaks. Likewise, the electron cannot have a μ greater than the maximum value, or else it would have been reflected at some smaller value of the magnetic field and thus could not contribute to the current density at z.

In its present form the calculation of $J_x(z)$ is quite difficult, principally because of the complicated dependence of ξ upon E and μ, coupled with the awkward limits of integration. This difficulty can be eliminated if it is realized that we are not interested in $J_x(z)$ directly, but rather in an integral of it over z as displayed in the expression for the power dissipation. Thus we choose to replace the independent set of variables z, E, μ with the set ξ, z_o, μ. Noting that

$$dz dE d\mu = \frac{2z_o}{L} B_o^{1/2} B^{1/2} \mu^{1/2} \left(\frac{E}{B} - \mu\right)^{1/2} dz_o d\xi d\mu, \tag{26}$$

we can write the power dissipation in the limit of vanishingly small imaginary part of the frequency as

$$\langle P_M \rangle = -\frac{1}{2}\left(\frac{e|E_o|}{m}\right)^2 \frac{\pi}{L}\left(\frac{2}{e}\right)^{1/2}\left(\frac{e}{m}\right) B_o^{1/2}\, \mathrm{Re} \int_0^\infty d\mu \int_0^{z_{max}} dz_o \int_0^{2\pi} d\xi \frac{B^{3/2} z_o \mu^{3/2} I'}{\omega_c^{1/2}} \times \left[\left(\frac{\partial f_o}{\partial \mu}\right) - \frac{z_o}{4\mu}\left(\frac{\partial f_o}{\partial z_o}\right)\right], \tag{27}$$

where now

$$f_o(\mu, E) = f_o\left[\mu, B_o\mu\left(1 + \frac{z_o^2}{L^2}\right)\right] \tag{28}$$

$$B = B_o\left(1 + \frac{z_o^2}{L^2}\cos^2\xi\right) \tag{29}$$

$$N = \frac{1}{4}\frac{\omega_{co}}{\omega_m}\frac{z_o^2}{L^2} \tag{30}$$

$$\omega_m = \left(\frac{2B_o}{m}\right)^{1/2}\frac{\mu^{1/2}}{L} \tag{31}$$

$$\bar{\omega}_c = \omega_{co}\left(1 + \frac{z_o^2}{2L^2}\right). \tag{32}$$

Note that in this expression (27) only B and the exponentials in I' are functions of ξ. In order to perform the integration over ξ we again make the approximation that $z_o^2/L^2 \ll 1$ so that B may be assumed constant and equal to its midplane value. The resulting expression for the power dissipation is

$$\frac{\langle P_M\rangle}{-\left(\frac{e}{m}\right)^2 |E_o|^2 \pi^2\left(\frac{2}{m}\right)^{1/2}\frac{B_o^{3/2}}{L}} = \mathrm{Im}\int_0^\infty d\mu \int_0^{z_{max}} dz_o\, z_o\mu^{3/2}\left[\frac{\partial f_o}{\partial\mu} - \frac{z_o}{4\mu}\frac{\partial f_o}{\partial z_o}\right]$$

$$\times \sum_{n=-\infty}^{\infty} J_n^2(N)\left[\frac{1}{\omega + \bar{\omega}_c + 2n\omega_m} + \frac{1}{\omega - \bar{\omega}_c - 2n\omega_m}\right], \tag{33}$$

where, to be consistent, we have also made the small z_o^2/L^2 approximation for $\bar{\omega}_c$, except in the resonant denominators where small changes in z_o^2/L^2 are important.

In order to proceed further, we now limit the form of the zero-order distribution functions to those whose midplane (z = 0) distribution can be expressed as

$$f_m\left(v_{\perp 0}^2, v_{11 0}^2\right) = n_o F_\perp\left(v_{\perp 0}^2\right) F_{11}\left(v_{11 0}^2\right), \tag{34}$$

where the distribution is normalized so that its integral over all midplane velocities equals the midplane density of electrons, n_o. It is easy to show that the zero-order distribution for such a midplane expression then becomes

$$f_o(\mu, z_o) = n_o F_\perp\left(\frac{2B_o\mu}{m}\right) F_{11}\left(\frac{2B_o\mu}{m}\frac{z_o^2}{L^2}\right). \tag{35}$$

It must also be realized that in any particular situation the zero-order distribution must be such that it does not violate our basic assumption that the electrons are not allowed to penetrate too deeply into the mirror. Limiting ourselves to such distributions, we are free to extend the upper limit on the z_o integration to infinity, realizing that the distribution function will preclude the existence of many electrons beyond z = L. With these considerations, the integral over z_o may be performed in the limit of a vanishingly small negative ω_i to yield the result

$$\begin{aligned}\frac{\langle P_M\rangle}{-\frac{\pi^3}{2}\epsilon_o\frac{\omega_{po}^2}{\omega_{co}}L|E_o|^2} = \sum_{n=-\infty}^{\infty}\int_0^\infty d\eta\,\eta^{3/2}\Big\{F'_\perp(\eta)\Big[&J_n^2\left(N_n^+\right)F_{11}\left(\eta_n^+\right)\mu_{-1}\left(y_n^+\right)\\ &+J_n^2\left(N_n^-\right)F_{11}\left(\eta y_n^-\right)\mu_{-1}\left(y_n^-\right)\Big]\\ &+\frac{1}{2}F_\perp(\eta)\Big[y_n^+J_n^2\left(N_n^+\right)F'_{11}\left(\eta y_n^+\right)\mu_{-1}\left(y_n^+\right)\\ &+y_n^-J_n^2\left(N_n^-\right)F'_{11}\left(\eta y_n^-\right)\mu_{-1}\left(y_n^-\right)\Big]\Big\},\end{aligned} \tag{36}$$

where

$$y_n^+ = \frac{2(\omega-2n\omega_m-\omega_{co})}{\omega_{co}} \tag{37}$$

$$y_n^- = \frac{-2(\omega+2n\omega_m+\omega_{co})}{\omega_{co}} \tag{38}$$

$$\omega_m = \frac{1/2}{L} \tag{39}$$

$$N_n^\pm = \frac{1}{4}\frac{\omega_{co}}{\omega_m}y_n^\pm \tag{40}$$

and $\mu_{-1}(x)$ is the unit step function defined by

$$\mu_{-1}(x) = \begin{cases} +1 & x > 0 \\ 0 & x < 0 \\ +1/2 & x = 0. \end{cases} \tag{41}$$

In this expression, the dummy variable η can be identified physically to equal $v_{\perp 0}^2$, where $v_{\perp 0}^2$ is the magnitude of the transverse velocity at the midplane, and $\omega_{po} = \left(\frac{e^2}{m}\frac{n_o}{\epsilon_o}\right)^{1/2}$ is the midplane plasma frequency.

Equation 36 is the desired result of our calculations. It represents the time-average power supplied by a uniform transverse RF electric field to the electrons along a particular flux tube in a parabolic magnetic mirror.

From the derivation, it is clear that the only electrons that contribute to this dissipation are those that are "resonant," in the sense that

$$\pm\omega - \bar{\omega}_c - 2n\omega_m = 0. \tag{42}$$

It is also clear from (36) that, for $z_o \ll L$, the contribution from these resonant electrons is stabilizing (dissipation) if $\frac{\partial f_o}{\partial \eta} < 0$, and is destabilizing when $\frac{\partial f_o}{\partial \eta} > 0$.

We are, at present, studying this equation to determine the frequency ranges and distribution functions for which the electrons make a net destabilizing contribution.

C. E. Speck, R. J. Briggs

References

1. C. E. Speck, "Experimental Study of Enhanced Cyclotron Radiation from an Electron-Cyclotron Resonance Discharge," Quarterly Progress Report No. 89, Research Laboratory of Electronics, M. I. T., April 15, 1968, pp. 177-178.
2. Ibid., p. 179, see Fig. XIII-2.
3. C. E. Speck and A. Bers, "Experimental Study of Enhanced Cyclotron Radiation from an Electron-Cyclotron Resonance Discharge," Quarterly Progress Report No. 90, Research Laboratory of Electronics, M. I. T., July 15, 1968, pp. 135-144.
4. C. E. Speck and A. Bers, "Identification of a High-Frequency Microinstability," Quarterly Progress Report No. 86, Research Laboratory of Electronics, M. I. T., July 15, 1967, pp. 195-199.
5. A. Bers, "Plasma Instabilities in a Resonant Cavity," Quarterly Progress Report No. 91, Research Laboratory of Electronics, M. I. T., October 15, 1968, pp. 182-185.

VI. PLASMAS AND CONTROLLED NUCLEAR FUSION*

C. Plasma Diagnostics

Academic and Research Staff

Prof. G. Bekefi
Prof. B. L. Wright

Graduate Students

E. V. George
J. K. Silk

1. OPTICAL MEASUREMENTS OF ION TEMPERATURE IN A COLLISIONLESS MICROWAVE-GENERATED PLASMA

Introduction

This report presents the results of measurements of the ion temperature in a collisionless Argon plasma generated by microwaves at the electron-cyclotron frequency. For the experiments described in this report the electron density varies from $2.5 \times 10^{11}/cm^3$ to $3 \times 10^{12}/cm^3$, and the electron temperature is in the range 5-15 eV. The plasma is excited by means of a coupling structure located in a nearly uniform field between two magnetic mirrors. The plasma apparatus has been described in previous reports.[1,2] The ion temperature is determined from measurements of the Doppler breadth of the 4610 Å Argon ion emission line by using a pressure-scanned Fabry-Perot interferometer.[3,4]

The ion temperature has been measured as a function of the externally controlled plasma conditions, such as pressure, magnetic field, and microwave power input. Observations have been made both transverse and parallel to the applied magnetic field. The data presented in the following paragraphs show that the ion temperature is approximately 0.2-0.3 eV independent of external conditions. The parallel ion temperature is roughly equal to the transverse temperature.

Experimental Results

The transverse ion temperature data are shown in Figs. VI-10 through VI-13. The measurements were made with the plasma viewed from the side as described previously.[3] The horizontal dashed line in each figure represents the average data. The error brackets indicate the effect of the uncertainty in the instrumental broadening only. When a more complete error analysis is performed true error brackets will be computed, including additional sources of uncertainty such as electronic noise. Meanwhile,

*This work was supported by the U.S. Atomic Energy Commission (Contract AT(30-1)-3980).

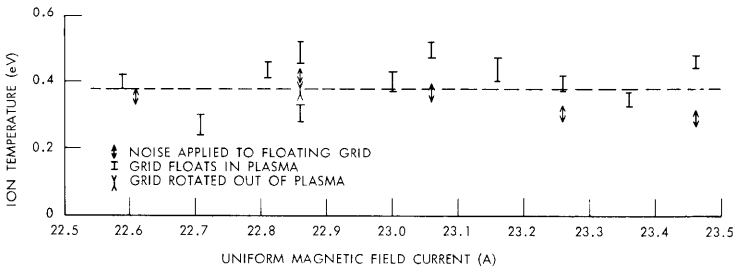

Fig. VI-10. Transverse ion temperature vs uniform magnetic field current. RF power, 54 W; mirror current, 65.3 A; pressure, 3.5×10^{-5} Torr.

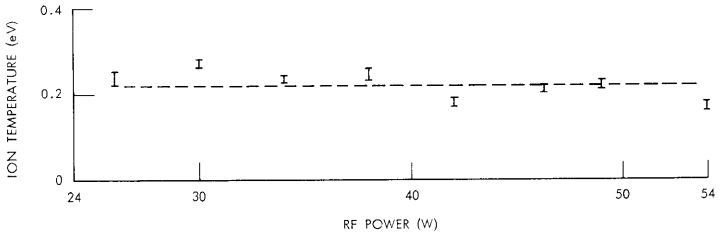

Fig. VI-11. Transverse ion temperature vs RF power. Mirror current, 65.4 A; uniform field current, 22.95 A; pressure, 3.6×10^{-5} Torr.

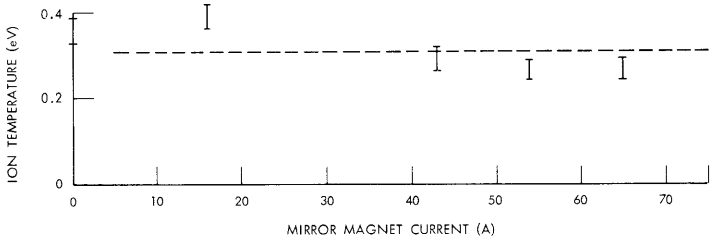

Fig. VI-12. Transverse ion temperature vs mirror magnet current. RF power, 52 W; pressure, 4.5×10^{-5} Torr.

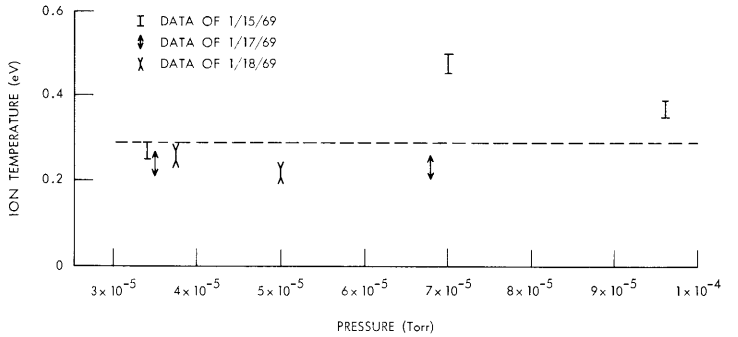

Fig. VI-13. Transverse ion temperature vs pressure. RF power, 46 W; mirror current, 65.58 A; uniform field current, 23.05 A.

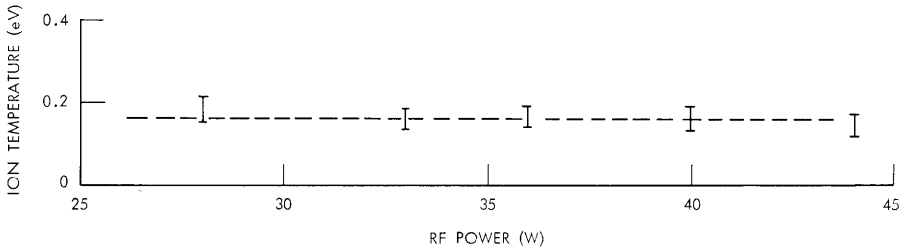

Fig. VI-14. Longitudinal ion temperature vs RF power. Mirror current, 66.26 A; uniform field current, 23.92 A; pressure 4.2×10^{-5} Torr.

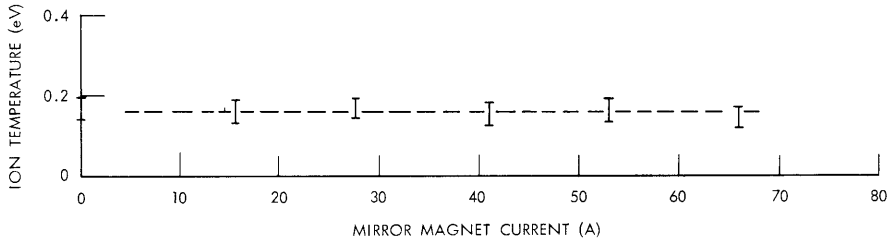

Fig. VI-15. Longitudinal ion temperature vs mirror magnet current. RF power, 44 W; pressure, 4.2×10^{-5} Torr.

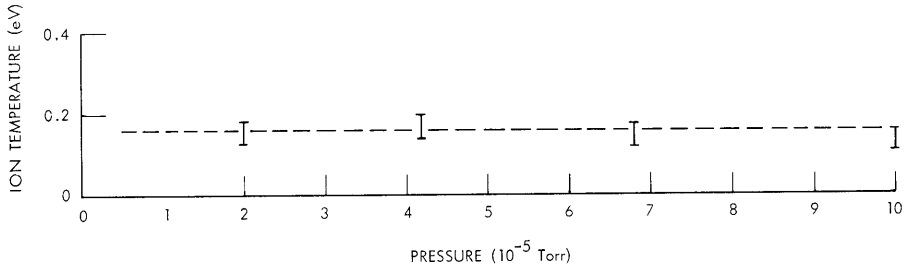

Fig. VI-16. Longitudinal ion temperature vs pressure. RF power, 44 W; mirror current 66.70 A; uniform field current, 23.56 A.

we plan to reduce the uncertainty in the instrument breadth by using a better calibration source.

Figure VI-10 indicates that the ion temperature is approximately 0.38 eV as the uniform magnetic field is varied approximately 4%. Outside this range the plasma is extinguished. The field at the midplane of the apparatus is approximately 1100 G at 23 A. Figure VI-10 also shows that the ion temperature does not change appreciably when a grid is introduced into the plasma. The grid is a 90% transmitting tungsten mesh disk of slightly greater diameter than the plasma. It is located 8 cm from the output of the plasma generating structure and is between the structure and the observation region. It can be moved completely out of the plasma column. Normally, the grid is allowed to float. Applying a 120 V peak-to-peak 0-20 kHz noise signal to the grid had no effect on the ion temperature, as shown in the figure.

Figure VI-11 indicates that the ion temperature is approximately 0.22 eV independent of the RF power between 26 W and 54 W. These results were obtained with the grid floating in the plasma.

Figure VI-12 shows the ion temperature to be roughly 0.31 eV independent of the mirror magnetic field. At a mirror current of 65 A the peak mirror field is approximately 1.8 kG. As the mirror current was reduced the uniform field was increased slightly (~4%) to maintain cyclotron resonance at the plasma-generating structure. These data were taken before the grid was installed. It is interesting to note that Langmuir probe measurements show that the electron density decreases by only a factor of two as the mirror field is reduced to zero.

In Fig. VI-13 the ion temperature is seen to be approximately 0.29 eV independent of pressure from 3.4×10^{-5} Torr to 9.6×10^{-5} Torr. The measurements were made before the installation of the grid.

The reproducibility of the data is somewhat unsatisfactory. There is some random scatter, as can be seen especially in Fig. VI-10. More perplexing are apparently systematic variations from one set of data to another. The average of all data shown in these figures is 0.32 eV, but all of the data in Fig. VI-11, for example, are consistently close to 0.22 eV, while the data in Fig. VI-10 are similarly clustered around 0.4 eV. On the other hand, Fig. VI-13 shows a case in which fairly good day-to-day repeatability was obtained. The reason for the imperfect reproducibility is not known. At present, the best statement that can be made to characterize the data is that the transverse ion temperature is 0.3 ± 0.1 eV independent of RF power, magnetic field, and pressure.

The longitudinal ion temperature data are shown in Figs. VI-14 through VI-16. To make these measurements, an optical mirror system was arranged so that the interferometer views the plasma column along its axis, through a window in the end of the cylindrical vacuum chamber far from the plasma-generating structure. A quarter-wave

plate and polarizer are used to exclude one of the two groups of circularly polarized Zeeman σ components of the line. The splitting within the group of components transmitted to the interferometer is negligible compared with the line breadth.

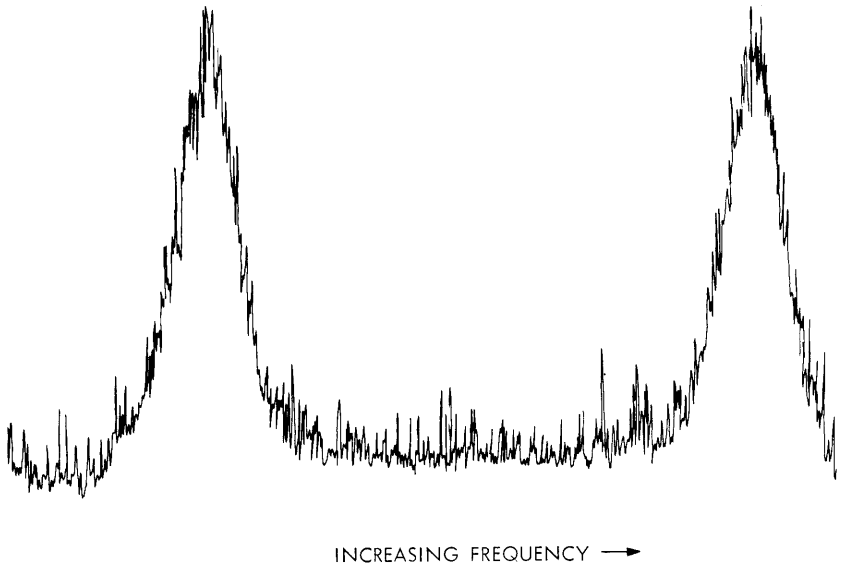

Fig. VI-17. Typical interferometer output trace-transverse view. RF power, 54 W; mirror current, 65.31 A; uniform field current, 22.95 A; pressure, 3.5×10^{-5} Torr.

As before, the dashed line in each figure represents the average data, and the error brackets indicate the effect of the uncertainty in instrument breadth. All measurements were made with the grid floating in the plasma.

Figure VI-14 shows that the longitudinal ion temperature is 0.16 eV independent of RF power. Figure VI-15 shows that the ion temperature does not change as the mirror magnet current goes from 0 to 67.5 A. Figure VI-16 indicates no variation in temperature with pressure between 2×10^{-5} Torr and 1×10^{-4} Torr. It is observed that the parallel ion temperature, like the transverse temperature, is independent of the external plasma conditions. The two temperatures are roughly equal.

A point of difference between the longitudinal and transverse measurements can be seen by comparing Figs. VI-17 and VI-18 which show typical measured line shapes observed in the transverse and parallel directions. In the transverse view the profile of the line is somewhat asymmetric: the low-frequency wing is brighter than the high-frequency wing. The direction of this effect is not changed by reversing the magnetic field. In the longtitudinal view the asymmetry is not seen. It is generally greatest in transverse measurements, which indicate higher than average temperatures. These observations suggest that when the plasma is viewed from the side,

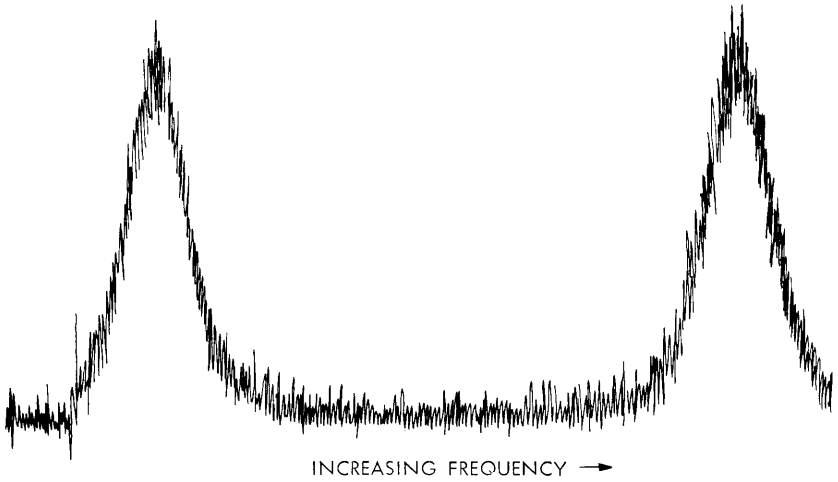

Fig. VI-18. Typical interferometer output trace-longitudinal view. RF power, 44 W; mirror current, 66.26 W; uniform field current, 23.92 A, pressure, 4.5×10^{-5} Torr.

nonthermal transverse motion has the effect of increasing the width of a line to slightly more than its purely thermal width. This possibility is consistent with the fact that a slightly lower temperature was measured in the longitudinal than in the transverse direction. It is evident that such an effect cannot be large compared with the thermal motion, however, because the transverse and parallel temperatures are nearly equal.

Plans for Further Work

Plans for the future include further study of the cause of the line asymmetry that was seen in the transverse observations. It is also necessary to improve the repeatability of the data. These two problems may be interrelated, since asymmetry and higher than average temperatures are associated. A distinct task involves comparison of wavelengths in transverse observations. The objective is to detect streaming motion along the axis of the plasma. Work on this measurement is now under way.

J. K. Silk

References

1. L. P. Mix, Jr., E. W. Fitzgerald, and G. Bekefi, Quarterly Progress Report No. 92, Research Laboratory of Electronics, M. I. T., January 15, 1969, pp. 227-236.
2. J. K. Silk, E. W. Fitzgerald, and G. Bekefi, Quarterly Progress Report No. 92, op. cit., pp. 258-264.
3. J. K. Silk, Quarterly Progress Report No. 92, op. cit., pp. 255-257.
4. J. K. Silk, Quarterly Progress Report No. 88, Research Laboratory of Electronics, M. I. T., January 15, 1968, pp. 149-152.

VI. PLASMAS AND CONTROLLED NUCLEAR FUSION*

D. Fusion-Related Studies

Academic and Research Staff

Prof. D. J. Rose
Prof. R. J. Briggs

Graduate Students

G. L. Flint, Jr.
Y. Y. Lau
A. E. Wright

1. HAZARDS OF TRITIUM FROM CONTROLLED FUSION

There has been some discussion[1,2] about the hazards that are likely to be enjoyed by the general public as tritium is inadvertently released, if power were generated by controlled fusion.

It has been concluded on qualitative bases that no great danger exists,[2] but the argument can be put more quantitatively. Suppose that all of the world's power – of every kind – were produced by nuclear fusion, and that the power level were the maximum permissible without warming the world unduly. That rate is approximately 10^{22} J/yr, approximately 1% of the total solar radiation incident on the earth. The fusion reaction D(T, n) α yields 17.6 MeV, and the companion tritium-breeding reaction Li^6(n, T) α yields 4.8 MeV. Thus the total energy released is 22.4 MeV/fusion, and we find that 2.8×10^{33} tritons/year must be bred. If all of these tritons were permitted to decay normally, there would be produced 2.4×10^{15} Ci/yr, and the steady-state inventory would be 4.3×10^{16} Ci world-wide.

Now refer to Jacobs,[3] who traces what happens to tritium that is released to the environment; he finds that 10^8 Ci of tritium would give a world-wide dose rate of 10^{-6} rem/year. According to the National Commission for Radiation Protection, the permissible dose level for the public should not exceed 0.5 rem/year from all causes. Because tritium cannot be allowed to make up the entire dose (but with these assumptions, what other substantial radiation source would there be?), the steady-state environmental inventory must be kept well below 5×10^{13} Ci.

All of this seems to suggest that the accepted fractional release of generated tritium should be kept well below 10^{-3}. In fact, because most of the fuel would be recycled through a fusion reactor and the burn-up per pass might be 0.1, an even more stringent requirement of well below 10^{-4} fractional loss per pass might be imagined. At present, nearly all of the tritium present in used fission fuel elements is released to the

*This work was supported by the U.S. Atomic Energy Commission (Contract AT(30-1)-3980).

environment, when the fuel is reprocessed.[3]

In fact, things do not look bad. Tritium from fission is released, at present, because it is a very minor product (atom yield $\approx 10^{-4}$/fission) and causes no trouble. In fission fuel element reprocessing, the released activity fraction is, at present, $\approx 10^{-6}$ or less. Also, the assumed conditions are the most extreme that could ever exist, and could not be realized for several hundred years, even if fusion should become fully feasible today. Thus, that amount of time would be available for us in which to set up moderately good housekeeping of tritium. Under the more credible assumption of 10^{20} J/yr world-wide (half the present total power rate) a loss of well below 10^{-2}/cycle would suffice. Any such high rate would be technologically preposterous.

Note that these fractions refer to tritium actually released to the environment, not just stored more or less irrecoverably in surcharged components. The scheme proposed by Fraas[4] for recovering tritium from a fusion reactor blanket lends itself to very low environmental loss; possibly, a similar scheme can be applied to the main plasma exhaust.

D. J. Rose

References

1. F. L. Parker, "Radioactive Wastes from Fusion Reactors," Science 159, 83-84 (1968).
2. F. L. Parker and D. J. Rose, "Wastes from Fusion Reactors," Science 159, 1376 (1968).
3. D. G. Jacobs, "Sources of Tritium and Its Behavior upon Release to the Environment," Report TID 24635, Clearinghouse for Federal Scientific and Technical Information, National Bureau of Standards, U. S. Department of Commerce, Springfield, Virginia 22151.
4. A. P. Fraas, "A Diffusion Process for Removing Tritium from the Blanket of a Thermonuclear Reactor," USAEC Report ORNL-TM-2358, Oak Ridge National Laboratory, December 1968.

2. PULSED FUSION DEVICES: WALL HEATING

Ribe has proposed[1] a pulsed fusion device with a 10-cm vacuum wall radius R_c and a maximum B field of 200 kG. The vacuum wall is the magnetic-field-producing coil and withstands the stress produced thereby. The plasma has a temperature of 15 keV, and a radius of half the wall radius. The burning time τ_T is 3/8 the field period τ, and a cooling mechanism operates between pulses.

In the present study we investigate the maximum surface temperature after each pulse in such a wall. The heating mechanisms considered are Bremsstrahlung, neutron, and electrical heating. During the burning time, the Bremsstrahlung power is deposited in a thin surface layer (approximately 2 mm). From the slab model

for a square pulse of Bremsstrahlung radiation of duration t, the temperature profile caused by Bremsstrahlung is given by

$$T_B(r,t) = \frac{1.83 \times 10^{-19}\, B^4 R_c}{K_v} \left\{ 2\sqrt{\frac{K_v t}{C_v \pi}}\, e^{-\frac{r^2 C_v}{4K_v t}} - r\ \mathrm{erfc}\left(\frac{r}{2\sqrt{\frac{K_v t}{C_v}}} \right) \right\},$$

where

K_v = thermal conductivity of the wall in W/cm °C

C_v = heat capacity per unit volume of the wall in J/cm^3 °C.

Since the neutron energy is deposited uniformly in the wall during the burning time, the neutron heating contribution to the temperature profile is

$$T_N(r,t) = 9.15 \times 10^{-19}\, B^4 R_c N_c \sigma E t / C_v,$$

where

N_c = number density of wall atoms

σE = mean cross section times energy deposited in the wall.

The electrical power is approximated by a constant power deposition with a spatial distribution of e^{-2r/δ_E}, where δ_E is the electrical skin depth for a sine pulse in the magnetic field at the operating temperature T_{op}. The temperature profile resulting from electrical heating is then given by

$$T_E(r,t) = \frac{8.34 \times 10^{-5}\, \eta^{1/2} B^2 t\, e^{-2r/\delta_E}}{C_v \tau^{1/2} \delta_E}.$$

Since the resistivity η is temperature-dependent, the electrical heating contribution to the temperature profile is found by an iterative procedure. Thus the maximum wall temperature during a pulse is given by

$$T_W \approx T_B(0, \tau_T) + T_N(0, \tau_T) + T_E\left(0, \frac{11}{6}\tau_T\right) + T_{op}.$$

Heating caused by synchrotron radiation is one thousandth that of Bremsstrahlung radiation and negligible in this device, since T_e is so low. Heating caused by gamma-ray backscattering is still to be considered.

A coil of copper-zirconium (0.15% zirconium) with a TZM backing to withstand the magnetic pressure has been considered. Since its electrical properties are approximately the same as those of copper,[2] the coil is treated as having the same heat-transfer properties as copper. The stress condition on the TZM with a safety factor of 2 and an operating temperature of 800°K determines the magnetic field. The maximum wall temperatures for this coil appear in Fig. VI-19 for various fractional burn-ups f_b which

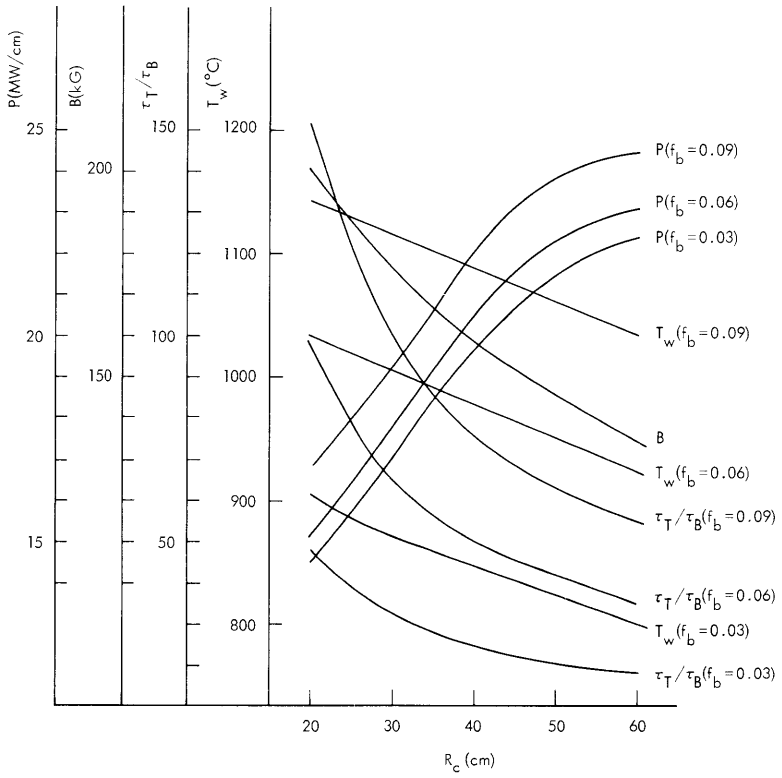

Fig. VI-19. Copper-zirconium coil.

determine τ_T. Approximately 70% of the rise over the ambient value comes from Bremsstrahlung, 10% from direct neutron scattering, and 20% from electric heating. The number of Bohm times needed to achieve τ_T is shown, as well as the usable power obtainable from this device during one pulse,

$$P = \frac{3\epsilon}{8} P_T + (\epsilon - 1) \frac{W_E}{\tau},$$

where

P_T = thermonuclear power

ϵ = efficiency of converting to usable power = 0.4

W_E = electrical energy deposited in the coil.

Note that the pumping power for the coolant has not been included. The copper-zirconium coil is not feasible, except possibly in a large machine with low power output.

Two other coils under consideration are niobium-zirconium (1% zirconium) and TZM (0.5% titanium, 0.1% zirconium, 99.4% molybdenum). The comparison of these coils with that of copper-zirconium for $f_b = 0.09$ is shown in Fig. VI-20. Niobium-zirconium is not feasible, because of loss of strength at these temperatures. The TZM

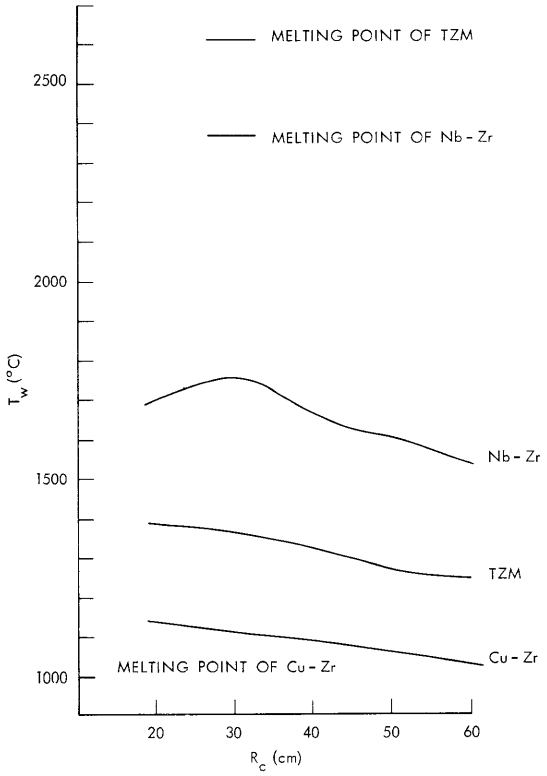

Fig. VI-20. Comparison of the niobium-zirconium, TZM, and copper-zirconium coils.

coil, despite its higher electrical heating, is the best of the three coils considered.

Further work is to be done on investigating operation at lower magnetic field; also to be studied is whether tritium can be regenerated in these systems. We expect that successful tritium breeding will require thinner coils than those considered in this report. This will lead to devices requiring less field and producing less power.

G. L. Flint

References

1. F. Ribe, "Feasibility Study of a Pulsed Thermonuclear Reactor," Report LA-3294-MS, Los Alamos Scientific Laboratory, Los Alamos, New Mexico, 1965.
2. A. E. Moredock and D. K. Fox, "Zirconium-Copper Alloy. High Strength and Conductivity," Metal Progress, April 1961.

3. EFFECT OF LOW FUEL BURN-UP IN PROPOSED DEUTERIUM-TRITIUM FUSION REACTORS

A computer study of conditions expected inside a deuterium-tritium (D-T) fusion reactor[1] is being extended to include the case of very low fractional fuel burn-up, and preliminary results have been obtained.

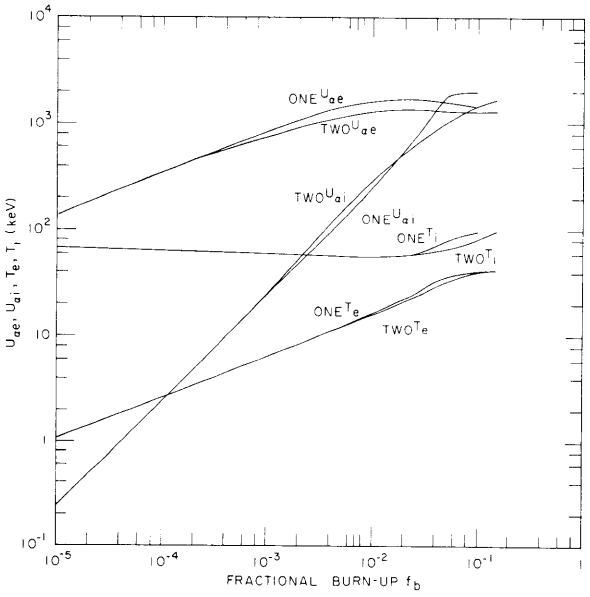

Fig. VI-21. Results.

In summary, the model is as follows: From Rose,[1] we use a proposed energy balance in the plasma. D and T ions are injected with energy V_i, for which power W_{si} is required. Inside the plasma, they have energies U_i in a presumed Maxwellian distribution at temperature T_i and density n_i. Ions are confined with a mean lifetime τ_i and carry off power W_{Li} as they leave. Similar things can happen to electrons, for which the symbols W_{se}, V_e, T_e, and W_{Le} apply. Furthermore, electrons can lose energy via Bremsstrahlung (W_x) and modified synchrotron radiation (W_c). Inside the plasma, D and T ions fuse, and two-tenths of the fusion power W_{DT} appears with the energetic helium nuclei (α particles, or α's) formed in the nuclear reaction. The α density, n_α, is small, but the energy, U_α, is high and hence the α pressure,

P_α, is substantial. The α's cool in the plasma by dynamical friction on both electrons and ions; their energy distribution is not Maxwellian. By assumption, the α's are also confined for a time τ_i. Finally, electrons and ions can interchange energy (W_{ei}).

Part of the D-T and electron heating in the plasma comes through heat transfer from the α's ($W_{i\alpha}$ and $W_{e\alpha}$); in a practical fusion reactor, this is necessary, so that the power inputs W_{se} and (especially) W_{si} can be kept acceptably low.

If the plasma confinement time τ_i is long enough, the heating problem is minimal: a fair fraction of the fuel (a fraction f_b for later reference) has time to react, and there is enough α energy available to heat the input D-T fuel. More than that, the α's are confined long enough to deposit their energy in the plasma before escaping. Detailed equations for the energy balance have been given by Rose[1]; solutions of them show that if f_b is approximately 0.04 or more, the α's deposit all of their energy in the plasma, even when plasma parameters T_e and T_i are relatively unfavorable for doing so.

The question under present study is: What happens when f_b is too small for the α's to be thermalized? This question is most important for proposed open-ended fusion systems, for which high ion temperature, T_i, is necessary for any reasonable confinement, and the energy cost of ion injection is correspondingly high. Table VI-1 shows some self-consistent plasma conditions calculated for typical open-ended systems. In every case, ions are injected at V_i = 100 keV, electrons are injected with zero energy (V_e = 0), the ion and electron confinement times are the same ($\tau_i = \tau_e$), and a (presumably) intermediate assumption is made about the escape of synchrotron radiation from the optically thick plasma. Besides symbols already defined, the table lists:

$n\tau_i$, an alternative measure of burn-up efficiency

ν = (α confinement time)/(α thermalization time) ($\equiv\theta/\phi$, see Rose[1])

$U_{\alpha e}$ = energy/fusion delivered to electrons

$U_{\alpha i}$ = energy/fusion delivered to ions

Q = (fusion energy)/(injection energy).

The trends are visible in Fig. VI-21, where the principal results are shown. At the left side of the figure, for negligibly small burn-up, each fusion event delivers only about 200 eV to the ions; even worse, the ion throughput is so large that each is heated only a few millivolts. Nevertheless, T_i = 66.7 keV, and $3T_i/2$ = 100 keV almost exactly, maintained by the injection energy (actually, the ions will not thermalize at such low burn-up, but we ignore that here). In marked contrast, $U_{\alpha e}$ = 130 keV, and electrons are heated to 1 keV by the α's. The thing to note on the left side of Fig. VI-21 is that when T_e and f_b are low, what little α heating of plasma there is goes to electrons.

Table VI-1. Parameters of hypothetical open-ended fusion system with low burn-up.

Case	1	2	3	4	5	6	7	8
f_b	9×10^{-6}	6×10^{-4}	3×10^{-3}	0.013	0.016	0.030	0.034	0.05
$n\tau_i$ (m^{-3} sec)	2×10^{16}	1.2×10^{18}	7×10^{18}	2.8×10^{19}	3.4×10^{19}	6.5×10^{19}	7.5×10^{19}	1×10^{20}
ν	9×10^{-3}	7.8×10^{-2}	0.22	0.47	0.53	0.76	0.83	>1
T_e (keV)	1.0	5.0	10.0	18.0	20	28	30	36
U_{ae} (keV)	132	675	1256	1705	1750	1776	1760	1649
T_i (keV)	65.67	61.8	58.1	57.0	57.6	63.7	66.3	80.6
U_{ai} (keV)	0.19	12.7	81	343	436	920	1083	1846
Q	8×10^{-4}	0.05	0.26	1.1	1.4	2.6	3.0	4.4

Table VI-2. Parameters of hypothetical open-ended fusion system with α's thermalizing by an exponential lifetime distribution.

Case	1	2	3	4	5	6	7	8	9	10	11
f_b	9×10^{-6}	6×10^{-4}	3×10^{-3}	.014	.018	.036	.042	.066	.095	.126	.154
$n\tau_i$ (m^{-3} sec)	2×10^{16}	1.2×10^{18}	7.3×10^{18}	3.0×10^{19}	3.8×10^{19}	7.8×10^{19}	9.2×10^{19}	1.5×10^{20}	2.2×10^{20}	3.1×10^{20}	4.1×10^{20}
ν	9×10^{-3}	7.8×10^{-2}	.22	.52	.59	.91	1.0	1.41	1.97	2.7	3.5
T_e (keV)	1.0	5.0	10.0	18.0	20.0	28.0	30.0	36.0	40.0	42.0	43.0
$U_{\alpha e}$ (keV)	130	617	1073	1367	1382	1364	1350	1313	1305	1317	1333
T_i (keV)	65.67	61.8	58.0	56.5	57.1	62.6	64.7	74.0	84.5	93.0	99.1
$U_{\alpha i}$ (keV)	0.20	13.5	96	405	493	843	930	1211	1443	1600	1707
Q	8×10^{-4}	.05	.3	1.2	1.5	3.2	3.7	5.8	8.5	11.0	13.6

As f_b rises to the range 10^{-2}-10^{-1}, $U_{\alpha i}$ rises, but not enough to raise T_i appreciably. In fact, T_i decreases slightly to 57 keV because the longer confinement time allows ions to lose more energy to the cool electrons.

As f_b rises above 0.02, there is a sharp change toward the operating conditions envisaged in an open-ended fusion system. $U_{\alpha e}$ saturates as T_e approaches 30 keV; the ions are heated substantially, and the α's have time to thermalize completely in the plasma. This is the region at the right side of Fig. VI-21, and is the region previously explored in detail.[1]

Other calculations were made, using an alternative assumption that α lifetimes have an exponential distribution, instead of one lifetime for all α's. Using an exponential lifetime τ_i, we obtained results to compare to calculations made under the one-lifetime assumption (see Table VI-2). In regions of low f_b, 10^{-5}-10^{-3}, the results are approximately equal to those of the other calculation. This gives some assurance of the insensitivity of the results, at least to some modest changes in the model, in regions of low burn-up. In regions of intermediate f_b, 10^{-3}-10^{-2}, T_e and T_i are approximately the same as before, but $U_{\alpha i}$ is slightly higher and $U_{\alpha e}$ is lower than before. This occurs because there are some α's in the exponential distribution that thermalize completely, thereby giving a higher fraction of total energy delivered to the ions and a smaller fraction to the electrons than occurs at incomplete thermalization. Also, $(U_{\alpha i} + U_{\alpha e})$ is smaller than before, since some α's will be lost quickly before much of their energy has been thermalized.

At higher f_b, greater than 10^{-2}, there are significant changes in the results. T_e, T_i, $U_{\alpha e}$, and $U_{\alpha i}$ drop below the values from the other assumption. This is because some α's escape before complete thermalization, whereas in the other assumption complete thermalization occurs at an f_b of slightly less than 0.05. Finally, at very high burn-up, the α's approach nearly complete thermalization, but T_e and T_i are still lowered because some α's escape with energy, and also on account of intense synchrotron radiation.

F. Marcus, D. J. Rose

References

1. D. J. Rose, "On the Feasibility of Power by Nuclear Fusion," Report ORNL-TM-2204, Oak Ridge National Laboratory, May 1968.

4. STABILITY OF A RELATIVISTIC ELECTRON LAYER

In a previous report,[1] we developed a model for the study of the stability of a relativistic electron ring guided by a uniform external magnetic field. In the present report, we shall derive from this model the dispersion relation for the negative-mass modes.

Previous work on the negative-mass instability[2,3] has been based on the assumption that the electron ring has an infinitesimal thickness. Our model enables us to extend the study to a finite beam. For simplicity, we take the electron density to be uniform between $r = r_1$ and $r = r_2$ (see Fig. VI-22). The differential equation for E_θ inside the beam is then

$$\frac{d}{dr}\left\{\frac{r}{\frac{\omega^2 r^2}{c^2} - \ell^2}\left[\frac{d}{dr}(rE_\theta) - \ell K E_\theta\right]\right\} + \frac{K\beta c}{\omega r - \ell\beta c}\frac{d}{dr}(rE_\theta) + E_\theta = 0. \tag{1}$$

In Eq. 1, $K = \omega_p^2/\omega\omega_o$, where ω_p is the electron plasma frequency, ω_o is the relativistic gyro frequency, and $\beta = v/c$. Note that K is constant for a uniform density profile, since

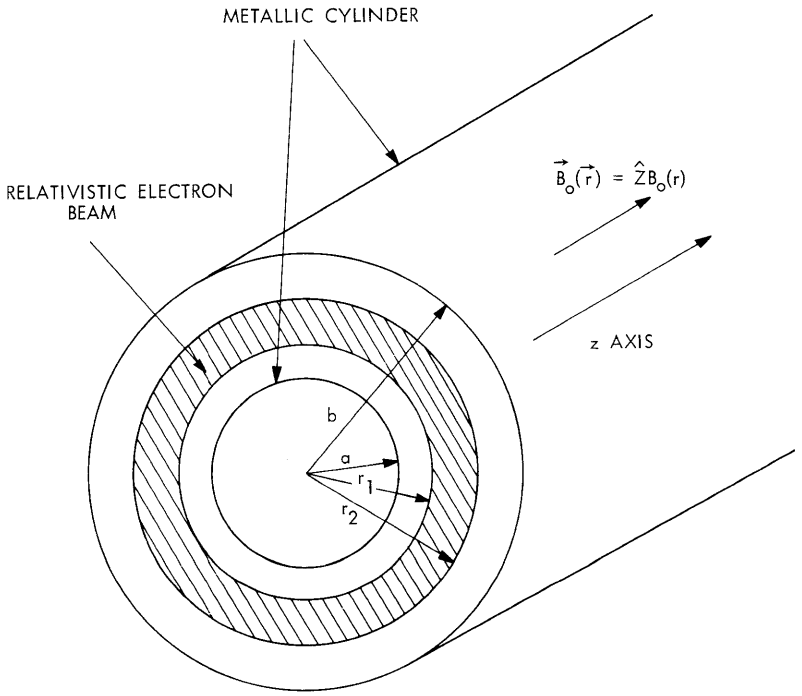

Fig. VI-22. The model. A layer of relativistic electrons, with density $n_o(r)$, is guided by a magnetic field $\vec{B}_o(\vec{r})$.

it is independent of the (radially dependent) relativistic mass.

In the limit of a sharp beam edge, we must allow for surface currents and charges in the boundary conditions. The value of the surface current K_θ can be readily determined from the expression for the volume current with a general profile, since $\left(\frac{\partial}{\partial r}\omega_p^2\right)$ becomes a delta function in the limit of a sharp beam edge. We have

$$K_\theta(r_1) = j\epsilon_o \frac{\omega_{p1}^2}{\Omega_1} r_1 E_{\theta 1}$$

and (2)

$$K_\theta(r_2) = j\epsilon_o \frac{\omega_{p2}^2}{\Omega_2} r_2 E_{\theta 2}.$$

Here (and henceforth, unless otherwise stated), we have used subscripts 1 and 2 to denote values at r_1 and r_2, respectively. We shall incorporate the effects of the vacuum region outside the beam by suitably defined wave admittances $b_\pm$, where

$$b_+ = \frac{\ell H_z\left(r=r_2^+\right)}{j\omega\epsilon_o r_2 E_\theta\left(r=r_2^+\right)}$$

$$b_- = \frac{-\ell H_z\left(r=r_1^-\right)}{j\omega\epsilon_o r_2 E_\theta\left(r=r_1^-\right)}. \tag{3}$$

The admittances b_+ and b_- depend only on the geometry of the container, and their values have been tabulated by Briggs and Neil[2] for various dimensions. From Eqs. 2 and 3 and the continuity of E_θ, we can write the boundary conditions at r_1 and r_2 as

$$\frac{\omega^2 r_1^2}{c^2} - \ell^2 \left[\frac{d}{dr}(rE_\theta) - \ell K E_\theta\right]_{r_1^+} = -r_1 E_{\theta 1} \left(\frac{b_-}{\ell} + \frac{\omega_{p1}^2}{\omega\Omega_1}\right) \tag{4}$$

and

$$\frac{\omega^2 r_2^2}{c^2} - \ell^2 \left[\frac{d}{dr}(rE_\theta) - \ell K E_\theta\right]_{r_2^-} = -r_2 E_{\theta 2} \left(\frac{b_+}{\ell} + \frac{\omega_{p2}^2}{\omega\Omega_2}\right). \tag{5}$$

Here we have represented H_z in terms of E_θ through Maxwell's equation.

The dispersion relation follows when the general solution of Eq. 1 is used in the boundary conditions above. Since Eq. 1 has no closed-form solution, we have considered the series solution to that equation. For a moderately thin beam, we should expect that only a few terms would provide a useful approximation.

Inspection of the differential equation reveals the fact that there are two regular singularities in the region of interest, namely at $r = r_a \equiv \frac{\ell c}{\omega}$ and at $r = r_s = \frac{\ell\beta c}{\omega}$. Since r_a

and r_s are regular singularities, solution of the form

$$\sum_{n=0}^{\infty} A_n(r-r_{a,s})^{n+\rho}$$

exists. We have proved that $\rho = 0, 1 + \frac{\ell K}{\gamma_o^2}$ when the solution is expanded about r_s, and $\rho = 0, 2$ about r_a. Therefore r_s is a branch point, and r_a may be a logarithmic singularity. The obvious question then arises whether the series solution expanded about one of the singularities will converge at the other, and hence at the boundaries. To answer this question, we must examine the solution about each of these singularities. We have shown that $r_a = \frac{\ell c}{\omega}$ is indeed an "apparent singularity" by the methods provided by Ince.[4] In other words, the solution to (1) expanded about r_a is analytic at that point. Therefore the solution expanded about r_s, the real singularity, converges at r_a, and hence at the boundaries r_1 and r_2. A series solution of the form

$$\phi \equiv rE_\theta = \sum_{n=0}^{\infty} A_n(r\omega-\ell\beta c)^n + \sum_{n=0}^{\infty} B_n(r\omega-\ell\beta c)^{n+\frac{\ell K}{\gamma_o^2}} \tag{6}$$

has been obtained. This series is not rapidly convergent, however, for a relativistic beam with $\gamma_o^2 \gg 1$. The dispersion relation obtained by taking the first three terms of the series solution provides us with a formidable amount of algebra but little information.

To obtain a dispersion relation for a relativistic beam with less complication, we set $\beta = 1$ and take $r_a = r_s$. In so doing, undoubtedly the solution in the immediate vicinity of the singularities will be drastically changed; however, as long as

$$|r_a - r_s| \approx \frac{|r_a|}{2\gamma_o^2} \ll r_2 - r_1 \equiv \tau, \tag{7}$$

the solutions at the boundaries should closely represent the actual solution with $\beta = 1$.

With $\beta = 1$ and

$$\phi = rE_\theta \tag{8}$$

$$\eta = \frac{\omega r}{c} - \ell, \tag{9}$$

Eq. 1 can be written

$$\frac{d^2\phi}{d\eta^2} + \frac{d\phi}{d\eta}\left[\frac{-(\eta^2+2\ell\eta+2\ell^2\eta^2) + K\eta(\eta+\ell)(\eta+2\ell)}{\eta(\eta+\ell)(\eta+2\ell)}\right] + \phi\left[\frac{2\ell K(\eta^2+2\eta\ell+\ell^2) + \eta^2(\eta+2\ell)^2}{(\eta+\ell)^2\cdot\eta(\eta+2\ell)}\right] = 0. \quad (10)$$

The solution about $\eta = 0$ is given by

$$\phi(\eta) = A\left[\eta^2 - \frac{1+3\ell K}{3\ell}\eta^3 + O(\eta^4)\right] + B\left[-K^2\eta^2 \log \eta + 1 + K\eta + O(\eta^3, \eta^3 \log \eta)\right]. \quad (11)$$

With (11) substituted in (4) and (5), we obtain the following dispersion relation

$$\frac{1}{\ell}(b_+ + b_-) + K\left(\frac{1}{\eta_1} - \frac{1}{\eta_2}\right) + K^2 \log\frac{\eta_2}{\eta_1} + K^2\left(\frac{\eta_1}{\eta_2} - \frac{\eta_2}{\eta_1}\right) + O(\eta, \log \eta) = 0.$$

Y. Y. Lau, R. J. Briggs

References

1. Y. Y. Lau and R. J. Briggs, Quarterly Progress Report No. 92, Research Laboratory of Electronics, M. I. T., January 15, 1969, pp. 266-271.
2. R. J. Briggs and V. K. Neil, "Negative-Mass Instability in a Cylindrical Layer of Relativistic Electrons," J. Nucl. Energy, Part C, Vol. 9, pp. 207-227, 1967.
3. V. K. Neil and W. Heckrotte, "Relation between Diochotron and Negative Mass Instabilities," J. Appl. Phys. 36, 2761 (1965).
4. E. L. Ince, Ordinary Differential Equations (Dover Publications, Inc., New York, 1956), pp. 396-408.